Geomorphology 413 (2022) 108351

Contents lists available at ScienceDirect

Geomorphology

journal homepage: www.journals.elsevier.com/geomorphology

Rock walls distribution and Holocene evolution in a mid-latitude mountain range (the Romanian Carpathians)

Mirela Vasile [a,*], Alfred Vespremeanu-Stroe [a,b], Daniela Pascal [b,c], Regis Braucher [d], Alin Pleșoianu [e], Răzvan Popescu [b], Bernd Etzelmüller [f], ASTER Team [d,1]

[a] GEODAR Research Group for Geomorphology, Geoarchaeology and Paleo-Environments, Research Institute of the University of Bucharest, 90-92 Sos. Panduri, 050663, sector 5, Bucharest, Romania
[b] Faculty of Geography, University of Bucharest, 1 N. Bălcescu Blv., 010041, sector 1, Bucharest, Romania
[c] Horia Hulubei National Institute for R&D in Physics and Nuclear Engineering, 30 Aleea Reactorului Str., 077125 Măgurele, Romania
[d] Aix-Marseille Univ., CEREGE, CNRS-IRD-Collége de France-INRAE, BP 80, 13545 Aix-en-Provence Cedex 4, France
[e] ESRI Romania, 25 Washington Str., sector 1, Bucharest, Romania
[f] Department of Geosciences, University of Oslo, 1047, Blindern, Oslo, Norway

ARTICLE INFO

Keywords:
Rock wall morphometry
Lithology
Rock slope failures
Cosmogenic nuclides
Romanian Carpathians

ABSTRACT

Rock walls in high mountain areas are the expression of long–term slopes response (10^3–10^5 years) to tectonics, weathering and denudation and a major source of sediment and hazard. Controls of mountain rock walls (RW) distribution and the response to post-glacial evolution are rarely discussed in the literature at the scale of mountain ranges. Using a database of 791 RW mapped in the Romanian Carpathians, we present their distribution and morphometry in respect to lithological classes, structural features and topography and relate their exposure to post–Younger Dryas (Holocene) rock slope failure chronology. Statistical analysis results show the high significance of structural and tectonic control on RW distribution, which prevails in sedimentary units where it imposed the predominance of West and North orientations and led to the formation of RW with dimensions up to a degree higher compared to other lithologies. Morphometric data indicate that metamorphic and igneous RW (linked to a great extent to glacial valleys and cirques headwalls) are usually restricted to the highest sectors of the mountain slopes, being characterized by reduced relative heights, asymmetrically distributed, common on the North-exposed slopes and extremely rare on the South. Based on 38 *in-situ* produced ^{10}Be surface exposure ages obtained on meter-sized boulders from the Southern and Eastern Carpathians, we hypothesise that metamorphic and igneous RW in the formerly glaciated Carpathian valleys were significantly shaped during Early Holocene (before 9 ka) by rock slope failures events that followed the deglaciation of the highest cirques and by intense RW permafrost degradation, which also affected some of the highest sedimentary units. We associate the long–term imprints of frost weathering to the significant North/South RW and rock glaciers distribution asymmetry, also identified in other mid-latitude mountain sites with similar topographic constraints.

1. Introduction

Open mountain RW are landforms highly sensitive for mechanical weathering and erosional processes (Hales and Roering, 2007; Matsuoka, 2008; Allen and Huggel, 2013; Phillips et al., 2017), the rates of which are dictated by the interplay of lithology, climate and the local uplift regime (Willett, 1999; Seong et al., 2009; Bartosch et al., 2017). Tectonics and structure significantly influence the extent and morphometry of the exposed rock surfaces in high mountain areas (Lifton et al., 2009; Ellis and Barnes, 2015; Sauchyn et al., 1998) which determine differential resistance to weathering and erosion, therefore it can be challenging to distinguish between the prevailing RW stability controls (Messenzehl and Dikau, 2017). Mountain RW are a continuous source area for geomorphic processes that trigger natural hazards like debris flows, rockfalls or rock avalanches especially when affected by permafrost degradation (Loye et al., 2009; Corona et al., 2013; Kromer, 2017). RW dynamics has been shown to be responsive to climate variables such as changes of permafrost conditions (Girard et al., 2013;

* Corresponding author at: Research Institute of the University of Bucharest, 90-92 Sos. Panduri, 050663, sector 5, Bucharest, Romania.
E-mail address: mirela.vasile@geo.unibuc.ro (M. Vasile).
[1] ASTER Team: Georges Aumaître, Karim Keddadouche, Fawzi Zaidi.

https://doi.org/10.1016/j.geomorph.2022.108351
Received 27 February 2022; Received in revised form 11 June 2022; Accepted 12 June 2022
Available online 15 June 2022

Krautblatter et al., 2013) and global climate change influencing periglacial processes (Gruber et al., 2004; Messenzehl et al., 2017; Phillips et al., 2017). In this context, additional information on the control factors that determine vertical RW distribution and (in)stability would contribute to improve knowledge on present and future mountain landforms responses to continuous warming, especially in mid-latitude ranges where permafrost is still preserved (Magnin et al., 2015), or is already in disequilibrium with the present climate (Vespremeanu-Stroe et al., 2012; Ardelean et al., 2017; Onaca et al., 2017a, 2020) and seasonal thawing prevails as rockfalls trigger (Onaca et al., 2015; Vasile and Vespremeanu-Stroe, 2017a).

Past RW response to climate changes during the Holocene has been consistently documented in the European and Scandinavian Alps, connecting RW failures magnitude and subsequent debris production to the post–Younger Dryas permafrost retreat (Hormes et al., 2008; Nagelisen et al., 2015; Hilger et al., 2021). In most of the formerly glaciated European mountain ranges, weathering and denudation rates are reported quantitatively after the Last Glacial period (Curry and Morris, 2004; Hughes et al., 2007; Messenzehl et al., 2017; Matthews et al., 2018). The occurrence of numerous rock slope failures (RSF) in response to local deglaciation debuttressing has been determined by absolute age dating (Soldati et al., 2004; Prager et al., 2008; Ballantyne et al., 2014) with time lags varying from immediate to millennial (Ballantyne et al., 2014). The reconstruction of RSF chronology in Tatra Mountains (Pánek et al., 2016) shows that low magnitude events occurring in high and steep topography hundreds of years after glacier retreat are likely triggered by ice mass disappearance, whereas complex RSF producing at millennial time–scale in lower topography of this range can also be associated with climate changing to warmer and more humid conditions during the onset of the Holocene and the Sub-Boreal period, highlighting the joint contribution of both ice disappearance and permafrost degradation in RW shaping and debris production. Additionally, absolute ages throughout the European ranges point to similar peak activity of RSF and deep-seated landslides in these time intervals (Soldati et al., 2004; Ivy-Ochs et al., 2009; Hermanns and Longva, 2013).

In this paper, we present a RW inventory at mountain range scale that covers multiple structural and lithological conditions of formerly glaciated and non-glaciated units of the Romanian Carpathians, which can still be considered hazard-prone areas. Based on RW morphometry analysis and geochronology, our main aim is twofold: i) to differentiate between the structural and climatic (glacial and periglacial) controls on RW distribution and ii) to evaluate long-term dynamics in this mid-latitude mountain range with potential implications to present RW stability. We provide a first insight on Holocene RSF occurrence as the last major shaping agent of RW in the Romanian Carpathians, filling a gap in the post-glacial chronology of Central-Eastern European mountain areas. The objectives are achieved by RW mapping and statistical analysis of morphometry parameters, and by in-situ ^{10}Be surface exposure data analysis in glacial cirques and valleys from five different massifs.

2. Study area

The Romanian Carpathians stand as a geographical subdivision of the Carpathian Mountain Arc that stretches in Central and Eastern Europe (44° 30′–47° 45′ N and 21° 30′–27° 10′ E). They expand to a length of 900 km and reach the maximum altitude of 2544 m above sea level (a.s.l.). The three main subdivisions (i.e., the Eastern and Southern Carpathians – abbreviated EC and SC further on – and the Apuseni Mountains, Fig. 1a) show lithological and topographic differences that reflect the complexity of the geological evolution, structural characteristics, and the influence of Pleistocene glaciations.

The Carpathians are part of the Alpine Orogeny and include tectonic units dating prior to the alpine event, in the Palaeozoic and early Mesozoic. The youngest exhumation phases determined by thermochronology age patterns in the central part of the SC are Latest Cretaceous – Middle Eocene (Merten, 2011; Matenco, 2017). The south–western sector of the SC underwent Oligocene – Miocene exhumation, whereas most of the EC correspond to Early – Middle Miocene phases, except for the SE Carpathians (Curvature Carpathians) which started uplifting in both Miocene and Latest Pliocene – Quaternary exhumation episodes (Merten, 2011). The EC are built on a central Crystalline Unit (correspondent to present Rodna, Maramureș, Rarău and Hășmaș Mts), Cretaceous Flysch (Ceahlău and Ciucaș Mts, extending towards the SC in Bucegi Mts) and Palaeogene Flysch (Table 1, Fig. 2). Internal volcanism during the Miocene led to the formation of EC volcanic massifs while the Pliocene – Quaternary comprised both a rapid uplift of 500–1000 m (which led to the formation of the most recent depression areas), and the strongest volcanic activity in the area (Săndulescu, 1984; Linzer et al., 1998; Mutihac, 2004). The SC are comprised of three major Crystalline Units: the Getic Overthrust Nappe (Șureanu, Căpățânii, Lotru, Cindrel, Godeanu Mts), the Supragetic Overthrust Nappe (Făgăraș and Iezer Mts) and the Danubian Nappes (Retezat and Parâng Mts), the latter being formed by granitic and granodioritic batholiths in their central areas and marginal limestone massifs (Figs. 1a, 2, Table 1).

Present neo–tectonic movements show a differential uplift trend of the Carpathian orogeny with mean values of 1–3 mm/yr, higher values up to 3–5 mm/yr reported in the Eastern Făgăraș, Bucegi Mts and the Curvature Carpathians which are associated with the activity from Vrancea seismic region (Hoeven et al., 2005).

The past glacial activity in the Carpathian area is expressed by well–preserved glacial cirques, valleys and associated rock walls (Mîndrescu et al., 2010b), most of which were modelled during Late Glacial Maximum (LGM) and Late Glacial cold phases (Popescu et al., 2017). Periglacial landforms are also widespread, with about 307 rock glaciers mapped in the Southern Carpathians, most of which are relict, and only 48 are presently considered intact (Onaca et al., 2017b).

The Romanian Carpathians are characterized by a temperate–continental climate, the mean annual air temperature (MAAT) ranging from −2 °C at 2500 m a.s.l. (Vf. Omu meteorological station) and −0.4 °C at 2190 m a.s.l. (Țarcu station) to 3 °C at 1577 m a.s.l. (Cozia station) (Fig. 1 for locations). Using a lapse rate of 0.63 °C/100 m, the 0 °C MAAT isotherm is around 2000 m a.s.l. on North–facing slopes and 2100 m a.s.l. on South–facing ones. Moisture is supplied by the West and SW dominating winds originating in the North–Atlantic and the Mediterranean, mean annual rainfall above 2000 m is 1100–1300 mm, snow cover reaches 1.5–2.0 m during January–March, and lasts in average 150–160 days per season (Micu et al., 2015). In-situ RW thermal monitoring above 2200 m a.s.l. (Vasile and Vespremeanu-Stroe, 2017a, 2017b) exhibits prolonged seasonal frost (140–150 days/season with potential frost penetration depths reaching 2 m), and mean annual rock temperatures (MART) of 0.5 °C on the North–exposed slopes. MART values 3–4 °C higher are registered on the southern slopes, where daily temperature oscillations prevail, and continuous freezing rarely sets within the temperature range −3…−8 °C, empirically stated as the freezing window prone for ice segregation (Girard et al., 2013; Duca et al., 2014). Permafrost presence in rock glaciers and talus slopes is considered limited to patches within the shadiest sectors of these landforms, especially North-exposed, as indicated by intensive thermal regime monitoring and geophysical surveys (Vespremeanu-Stroe et al., 2012; Ardelean et al., 2017; Onaca et al., 2017b).

3. Methods and data

3.1. Rock wall mapping

RW were mapped based on the available time records of Google Earth satellite imagery. Because some images were not clear enough for a good differentiation between the RW and the adjacent geomorphological units, a comparison with higher resolution air photography was undertaken (orthophoto images available for view only from the

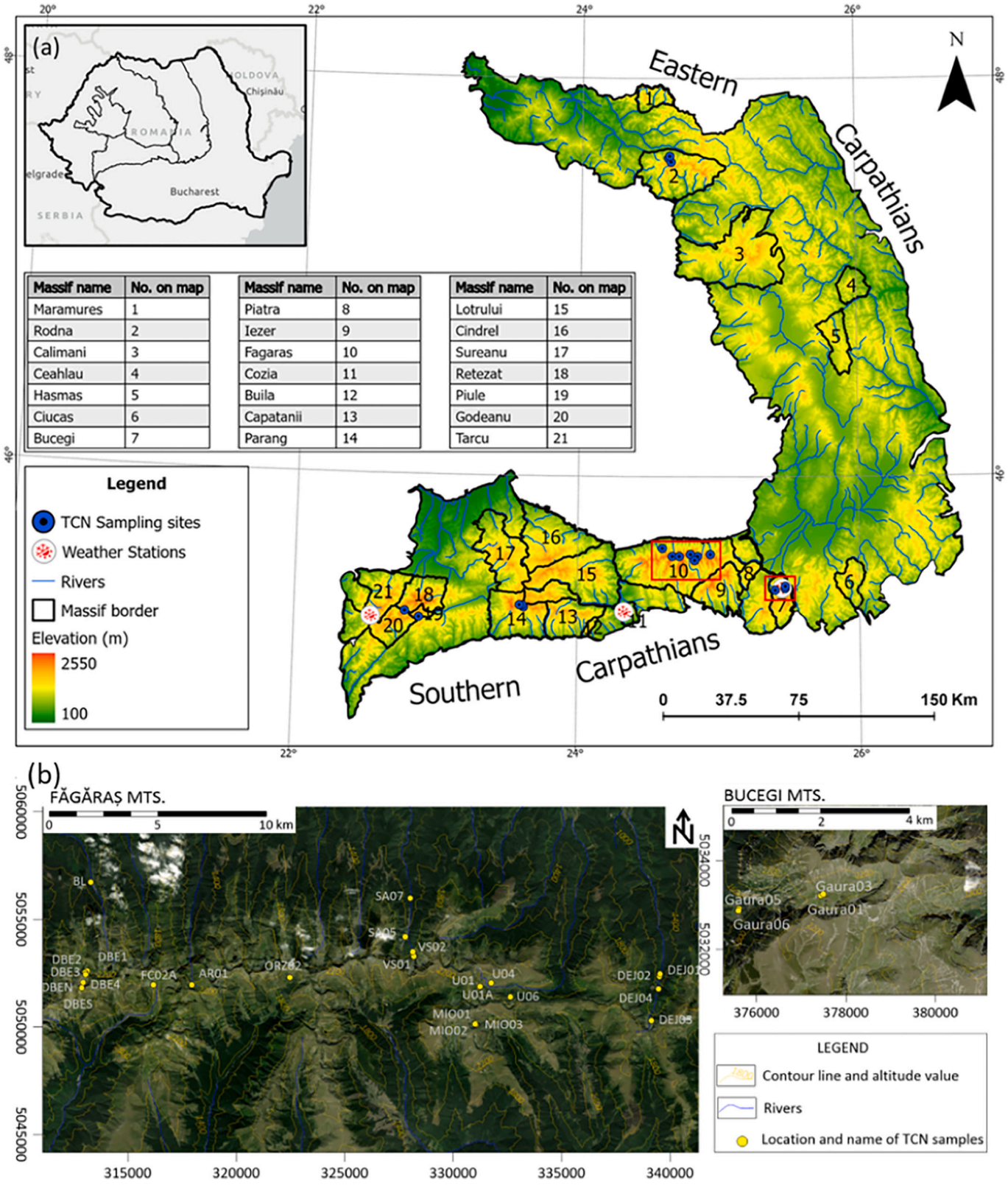

Massif name	No. on map
Maramures	1
Rodna	2
Calimani	3
Ceahlau	4
Hasmas	5
Ciucas	6
Bucegi	7

Massif name	No. on map
Piatra	8
Iezer	9
Fagaras	10
Cozia	11
Buila	12
Capatanii	13
Parang	14

Massif name	No. on map
Lotrului	15
Cindrel	16
Sureanu	17
Retezat	18
Piule	19
Godeanu	20
Tarcu	21

Fig. 1. (a) Carpathian Arc position in Romania (Eastern and Southern Carpathians, Apuseni Mts); Outline of the units included in the RW inventory (digital elevation by 1 arc-second resolution ASTER GDEM), location of meteorological stations in the Carpathians and of the sampling sites (valley/cirque) of absolute ages used in RSF geochronological reconstruction from Bucegi and Făgăraș Mts. (this study), Rodna Mts. (Gheorghiu, 2012), Parâng Mts. (Gheorghiu et al., 2015) and Retezat Mts. (Reuther et al., 2007; Ruszkiczay-Rüdiger et al., 2021). Red rectangles mark the areas represented in subplot b; (b) Distribution of boulders sampled for Terrestrial Cosmogenic nuclides (TCN) surface dating in Făgăraș and Bucegi Mts. in this study (coordinates are in UTM projection). (For interpretation of the references to colour in this figure legend, the reader is referred to the web version of this article.)

Table 1
Main lithological, structural and morphographic characteristics of the mountain units in which rock walls were mapped.

	Unit name (max. altitude)	Lithology /structure[a]	Extent/direction	Nr. of mapped RW	Glaciation[b]
Eastern Carpathians	Maramureş (1956 m)	Crystalline schist with peripheral limestone and sandstones Volcanic intrusions (basalts)	15 km long/NW–SE ridge	11	Yes
	Rodna (2303 m)	Crystalline schist, micaschists and paragneiss Horst, Dragoş Vodă Fault	40 km long/E–W ridge	19	Yes
	Călimani (2100 m)	Andesites (volcanic) Eroded craters	Volcanic cone	5	Yes
	Ceahlău (1969 m)	Conglomerates and flysch Suspended syncline	15 km/N–S	10	No
	Hăşmaş (1973 m)	Massive limestone West oriented syncline	3.5 km long/NW–SE ridge	6	No
	Ciucaş (1954 m)	Conglomerates and sandstones, flysch East oriented syncline	Two separated ridges 7 km/SW–NE and 3 km/NW–SE	37	No
Southern Carpathians	Bucegi (2505 m)	Conglomerates, sandstones Limestone with radiolarites N-S syncline, East oriented cuesta front slope	Reversed U–shape 30 km long ridge	49	Yes
	Piatra Craiului (2238 m)	Limestone with radiolarites Hogback	25 km long/NNE–SSW ridge	13	No
	Iezer (2459 m)	Micaschists and paragneiss Supragetic overthrust nappe	20 km long/SW–NE ridge	27	Yes
	Făgăraş (2544 m)	Micashists and paragneiss, amphibolite Supragetic overthrust nappe Northern–Făgăraş Fault Line	70 km long W–E ridge, and multiple secondary N-S ridges	248	Yes
	Cozia (1668 m)	Gneiss Horst	~70 km^2 surface	3	No
	Buila–Vânturariţa (1885 m)	Massive Limestone Hogback	14 km long/SW–NE ridge	23	No
	Parâng (2519 m)	Granitoids Amphibolite (Danubian Unit)	25 km long/E–W ridge	40	Yes
	Şureanu/Cindrel/Căpăţânii/ Lotrului (2130–2244 m)	Micaschists and paragneiss, amphibolite (Getic unit)	15–25 km long/E–W ridges	8/10/4/5	Yes
	Retezat (2509 m)	Granodiorite intrusions Crystalline schist, amphibolite (Danubian unit)	15 km long main/W–E ridge 2–5 km secondary N-S ridges	187	Yes
	Ţarcu (2196 m)	Conglomerates, sandstones, crystalline limestone Crystalline schist	20 km long/N-S then NE–SW ridge	26	Yes
	Godeanu/Piule Iorgovanul (2291 m)	Micaschists and paragneiss, amphibolite/recifal limestone	20 km long/NE–SW ridge	26/13	Yes
	Cerna Valley (1200 m)	Recifal limestone Graben	80 km long valley/NS	21	No

[a] According to the Geological Map of Romania, scale 1:200,000 (Geological Institute of Romania).
[b] According to the Map of Glacial Cirques in the Romanian Carpathians (Mîndrescu, 2016).

National Agency for Cadastre and Land Legislation at 1–5 m resolution, ANCPI). Further, the 25 m resolution EU–DEM digital surface model (European Environment Agency) was used to check slopes inclination and the inflection points within longitudinal profiles at the contact with the talus or at the top of the glacial cirques. The term rock wall refers herein to steep, bare and compact rock surfaces, situated above treelines, with angles usually higher than 37–40° (Gruber, 2007). We took into account RW with areas larger than 200 m^2 in order to avoid patchy rock surfaces partially covered with vegetation or sporadic discontinuous outcrops. Considering these constraints, the analysis is reduced to 21 mountain units from the EC and the SC (Fig. 1b), where rock surfaces matching these criteria were identified on satellite imagery. The geological map of Romania (scale 1: 200,000, Geological Institute of Romania) was used to determine the rock type of each mapped RW, assuring a complete spatial coverage over the entire range.

3.2. Rock wall morphometry

Mean RW area, total coverage, altitude, relative height, orientation and slope values were computed for each mountain unit (Table 2) and per lithology types, using the values from all units developed on the same rock class (sedimentary, igneous, metamorphic or volcanic). Each RW was vectorized and the resulting polygons were overlaid on the DEMs and then used for calculating the morphometric parameters in ArcGIS software. The averaging of aspect (orientation) values was done using circular statistics from 'circular' package implemented in R. The RW area was calculated for a 2D projection of the RW polygons on the EU–DEM.

3.3. Statistical analysis

The statistical analysis was performed in RStudio (R version 3.4.0), and consisted in three stages. First, a data normality check was performed using the Shapiro–Wilk normality test (Shapiro and Wilk, 1965), which indicated the non-normality of the data. Then, for each mountain unit, a Kruskal–Wallis one–way analysis of variance test (Kruskal and Wallis, 1952) was performed in order to check if there are any statistically significant differences between groups of quantitative parameters, namely the relations between exposures and morphometry, and between lithology and morphometry. The Kruskal-Wallis Test is the non-parametric alternative to ANOVA (one-way analysis of variance), which checks if the analysed groups are subsets from the same population. The computed H statistic then indicates whether the groups come from the same population by comparing it to a critical value, which for our analysis corresponds to a 95 % confidence or a p-value < 0.05. For H values beyond the critical threshold the Kruskal-Wallis Test indicates strong differences between analysed groups. Finally a post–hoc Dunn's Test (Dunn, 1961) for multiple comparisons was performed in order to

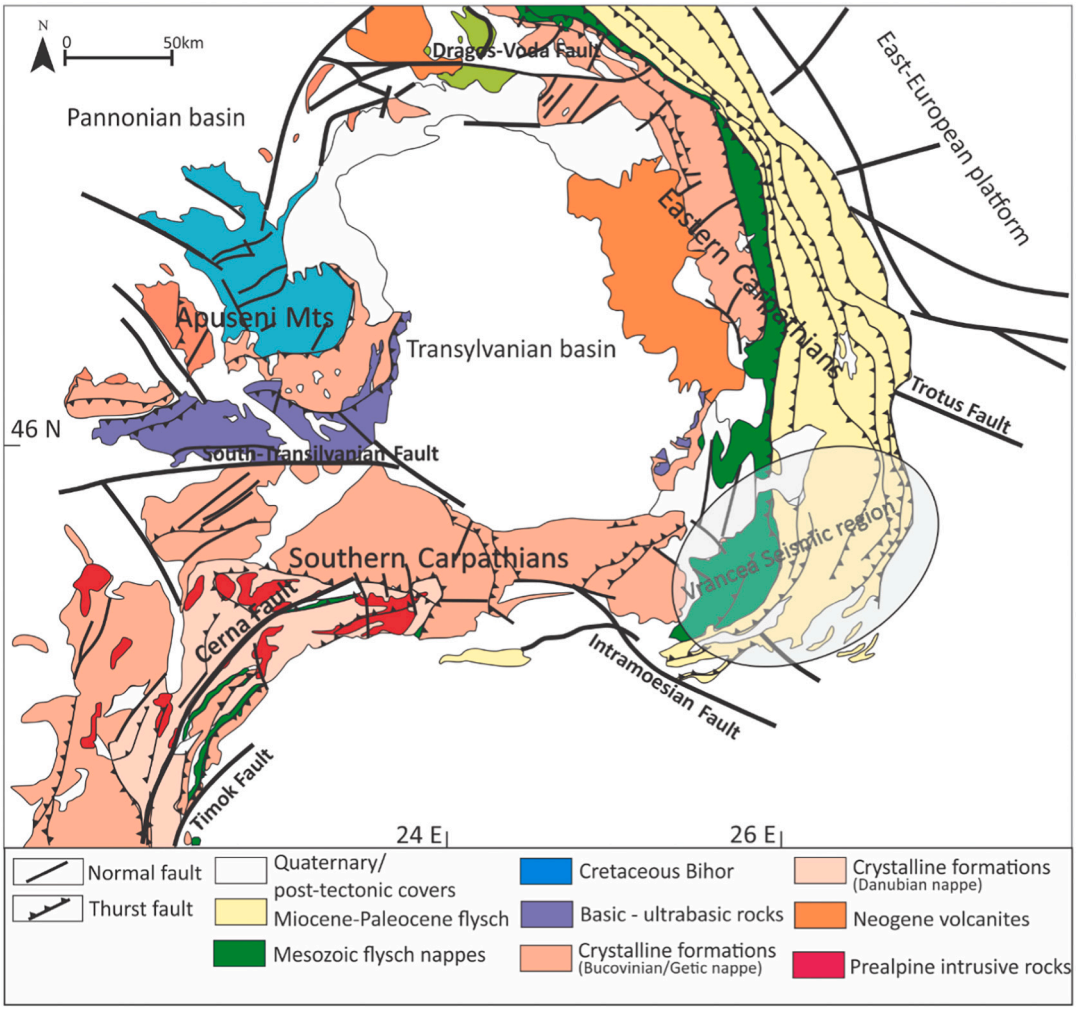

Fig. 2. Simplified geological map of the Carpathians and major fault lines (modified and adapted from Vaida and Verniers, 2005, and Merten, 2011).

Table 2
The averaged values of the morphometric parameters and total cumulated area of the mapped RW in EC and SC.

	Units	Main rock types	RW count	Mean RW area ($m^2 \times 10^3$)	Cumulated RW area ($m^2 \times 10^3$)	Mean height (m)	Mean slope (degrees)	Mean alt (m)
Eastern C.	Călimani	Volcanic	5	4.79	23.97	35.8	39	1984
	Ceahlău/Hășmaș/Ciucaș	Limestone	6	59.45	356.71	162.5	44	1546
		Conglomerate	47	41.82	1965.95	83.5	35	1645
	Maramureș/Rodna	Schist	24	15.81	379.55	55.4	44	1950
		Volcanic	6	7.60	45.63	69.7	38	1799
Southern C.	Bucegi	Conglomerate	42	116.16	4878.94	221.1	46	2096
		Limestone	7	72,5	507.51	175.5	48	1935
	Piatra Craiului	Limestone	13	220.82	2870.74	266.5	44	1967
	Făgăraș/Iezer	Schist	275	8.0	2200.78	73.1	41	2200
	Parâng/Retezat	Granite	175	12.5	2162.87	68.0	38	2229
		Schist	52	22,94	1193.22	95.7	40	2169
	Buila/Piule-Iorgovanul/Țarcu/	Limestone	70	34.1	1909.46	124.2	46	1346
	Cerna Valley	Conglomerate	17	14.38	244.47	59.3	41	1748
		Schist	8	8.75	70.04	65.3	46	1666
		Volcanic	2	4.83	9.67	46.0	39	1967
	Cozia/Cindrel/Șureanu/Lotrului/ Căpățânii/Godeanu	Schist	56	4.61	258.25	33.0	38	1916

identify which mountain units have significantly different values of each pair of the analysed parameters.

3.4. Surface exposure ages

24 boulders (20 from Făgăraș and four from Bucegi Mts) were sampled for cosmogenic ^{10}Be exposure dating. The samples are part of an extensive study regarding deglaciation and RSF, which counts >120 rock surfaces (unpublished data). During sample processing, the abundance of post–Younger Dryas resulting ages raised our questions about RSF triggering the detachment of such boulders, as documented in other European mountain ranges (synthesis of studies in Pánek et al., 2016). The samples included in the present study were collected along 7 glacial valleys in Făgăraș Mts and one valley in Bucegi Mts, ranging from 1205 to 2287 m a.s.l., on meter–sized boulders from both valley/cirque centre and peripheral (examples in Fig. 3). Sample size varied from 2 to 3 cm thick and sampled rock surfaces were vegetation free. We additionally took into account other 14 post–Younger Dryas absolute ages previously presented in deglaciation chronology studies from Rodna (Gheorghiu, 2012), Parâng (Gheorghiu et al., 2015) and Retezat massifs (Reuther et al., 2007; Ruszkiczay-Rüdiger et al., 2021).

Secondary, we aimed for absolute dating of a rock glacier (Doamnei RG) surface in Făgăraș Mts, where we sampled four boulders from the RG body on a longitudinal profile but also the source RW area above; for comparing a North/South RW exposure, the corresponding South–face of Doamnei RW was sampled.

The purification for Făgăraș and Bucegi samples following the procedure of Merchel and Herpers, 1999 was performed at *Laboratoire National des Nucléides Cosmogéniques* (LN2C) at CEREGE (Aix en Provence, France). Samples were crushed and sieved to the 0.25–1 mm fraction. Magnetic separation was performed on all samples with a magnetic separator "Frantz LB-1". The other minerals that are embedded in samples were eliminated with mixtures of HCl and H_2SiF_6. Then atmospheric ^{10}Be was eliminated by HF (48 %) dissolutions. Before the total dissolution, 150 mg of a ^{9}Be carrier solution (concentration 3025 ± 9 μg/g; Merchel et al., 2008) manufactured in-house from a phenakite crystal were added to the samples. The total dissolution of quartz was performed with HF 48 % (3.6 mL per g of quartz and 30 mL in excess). The resulting solutions were evaporated until dryness and samples were recovered with hydrochloric acid. Subsequently samples were precipitated with ammonia before successive separations through an anion exchange column (Dowex 1 × 8) to remove iron and a cation exchange column (Dowex 50WX8), and to discard boron and recover Be (Merchel and Herpers, 1999). BeO targets were prepared by mixing Niobium powder with the BeO oxide for AMS measurements at *ASTER, the French National AMS Facility* (CEREGE, Aix en Provence). The ^{10}Be measurements were calibrated against an In-House standard (STD11) Braucher et al., 2015, using an assigned ^{10}Be/^{9}Be ratio of (1.191) × 10^{-11} (1.09 %). Analytical uncertainties (reported as 1σ) included for all samples the counting statistics, the machine stability for the batch and an external uncertainty of 0.5 % (Arnold et al., 2010). Mean ^{10}Be/^{9}Be blank ratios were 3.30 ± 0.50 × 10^{-15}. The ^{10}Be half-life of (1.387 ± 0.01) × 10^{6} years (Chmeleff et al., 2010) was used.

Production rates were scaled following Stone, 2000 with a sea level high latitude production rate of 4.02 ± 0.36 atoms/g SiO_2/yr (Borchers et al., 2016). Rock density of 2.5 g/cm^3 was used for all samples. Topographic shielding was calculated using the CosmoCalc 2.2 Excel add-in of Vermeesch, 2007. Air pressure used is 1013 mBar. There was

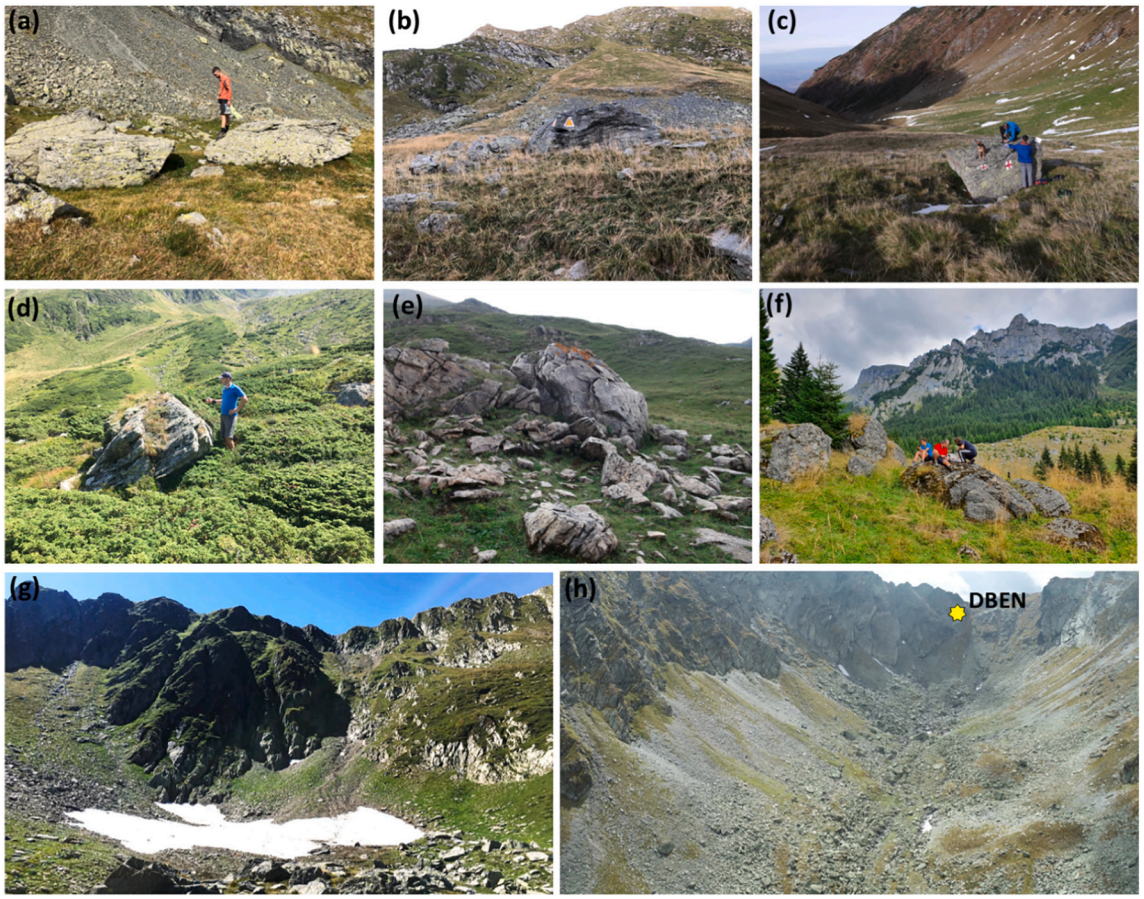

Fig. 3. Examples of TCN-dated boulders in Făgăraș (a, b – Fundul Caprei Valley; c, d – Sâmbăta Valley; e – Urlea cirque) and Bucegi Mts (f – Gaura Valley), Mioarele cirque headwall (g) and Doamnei cirque and rock glacier (h). Yellow dot in subplot (h) marks Doamnei North RW sampling spot for ^{10}Be surface exposure dating (see Table 5). (For interpretation of the references to colour in this figure legend, the reader is referred to the web version of this article.)

no quantitative information on the snow cover during the surface exposure duration, hence, no corrections for potential effects of snow cover or denudation were applied to the ages. ^{10}Be exposure ages were calculated following Eq. (1) using muogenic contributions of Braucher et al., 2011.

$$N(x,\varepsilon,t) = \frac{P_{sp}{*}exp\left(-\frac{x}{L_n}\right)\left(1-exp\left(-t\left(\frac{\varepsilon}{L_n}+\lambda\right)\right)\right.}{\frac{\varepsilon}{L_n}+\lambda} + \frac{P_{\mu slow}{*}exp\left(-\frac{x}{L_{\mu slow}}\right)\left(1-exp\left(-t\left(\frac{\varepsilon}{L_{\mu slow}}+\lambda\right)\right)\right.}{\frac{\varepsilon}{L_{\mu slow}}+\lambda} + \frac{P_{\mu fast}{*}exp\left(-\frac{x}{L_{\mu fast}}\right)\left(1-exp\left(-t\left(\frac{\varepsilon}{L_{\mu fast}}+\lambda\right)\right)\right.}{\frac{\varepsilon}{L_{\mu fast}}+\lambda} \quad (1)$$

where:

N (x, ε, t) is the nuclide concentration function of depth x (g/cm^2), denudation rate ε (g/cm^2/y) and exposure time t(y). P_{sp}, $P_{\mu slow}$, $P_{\mu fast}$ and L_n, $L_{\mu slow}$, $L_{\mu fast}$ are the production rates and attenuation lengths of neutrons, slow muons and fast muons, respectively. L_n, $L_{\mu slow}$, $L_{\mu fast}$ values used are 160, 1500 and 4320 g/cm^2, respectively (Braucher et al., 2003). λ is the radioactive decay constant. $P_{\mu slow}$, $P_{\mu fast}$ are based on Braucher et al., 2011.

4. Results

4.1. RW distribution

A total of 791 RW were identified and considered as individual features, most of which were mapped in the SC. In most of the mountain units considered here, the main ridges follow East–West or NE–SW direction (Table 1), tracking the principal fault lines (Fig. 2). The distribution of the RW is further presented in both formerly glaciated and non-glaciated mountain units, based on mean orientation and RW altitude. From the 21 units considered in this study, 11 preserve glacial landforms (Table 1). The best preserved landforms are in Făgăraș Mts, where 207 glacial cirques were mapped (Mîndrescu et al., 2010a, 2010b), in Retezat Mts, which show extensive moraine deposits, glacial lakes and complex glacial valleys (Urdea, 2000), and in Parâng Mts, which keep the largest glacial cirques in the Romanian Carpathians (Iancu, 1970). In the EC, only Rodnei, Maramureș, and Călimani massifs present visible glacial landforms (cirques, valleys and moraine deposits), most of which are in Rodnei Mts (Mîndrescu, 2016).

The RW mapped in the schist–prevailing massifs from the EC are distributed mainly on NE (23 %) and secondary on North and East (Fig. 4a) with an average altitude of 1950 m a.s.l. The andesitic and basaltic rock outcrops mapped in the EC, are largely grouped on the North and NE similarly with the metamorphic ones.

In the sedimentary units, RW extend on all orientations, with a maximum frequency on the South (almost 40 %) while 7 % were mapped on the northern slopes (Fig. 4b), but are limited to altitudes below 1800 m, reaching an average of 1634 m a.s.l. which is considerably lower (>300 m) than the metamorphic and volcanic RW.

In the SC, the number of RW built on metamorphic rocks is much larger than in the EC, most of which being distributed in two large massifs (Făgăraș and Iezer), and the remaining are spread in 6 units characterized by gentler topography and lower altitude (Fig. 5a, Table 2). The northern exposure clearly dominates in both clusters, summing 41 % from the total RW number, with similar frequencies on the NW and NE bins (Fig. 5d). The second highest RW frequency corresponds to the eastern orientation, followed by the western slopes. RW mapped on the southern slopes are scarce and represent only 5.4 % from the total number. In the large metamorphic massifs (Făgăraș and Iezer) the highest RW density is in the range of 2100–2400 m with a mean altitude of 2200 m (Table 2), but very few surfaces were mapped higher than 2400 m.

Parâng and Retezat Mts in the SC (Fig. 1a for location) are two examples of mixed lithology, being composed mainly of granitoids plus granodiorites intrusions and of crystalline schist, micaschist,

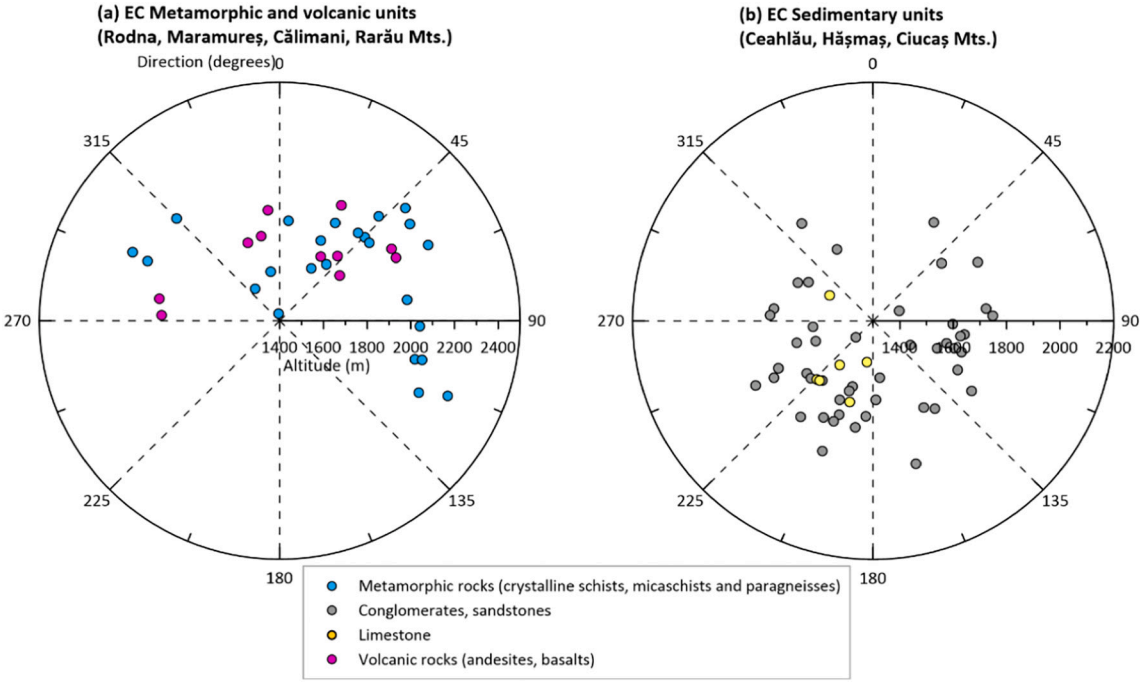

Fig. 4. Direction and mean altitude of the RW mapped in the EC: (a) the metamorphic schists prevailing units; the andesitic and basaltic outcrops are represented as volcanic RW; (b) the sedimentary units (limestone and conglomerates prevailing). The radius of the graphs represents the altitude values, the general direction is expressed in sexagesimal degrees and each dot represents a RW (please refer to the colour version).

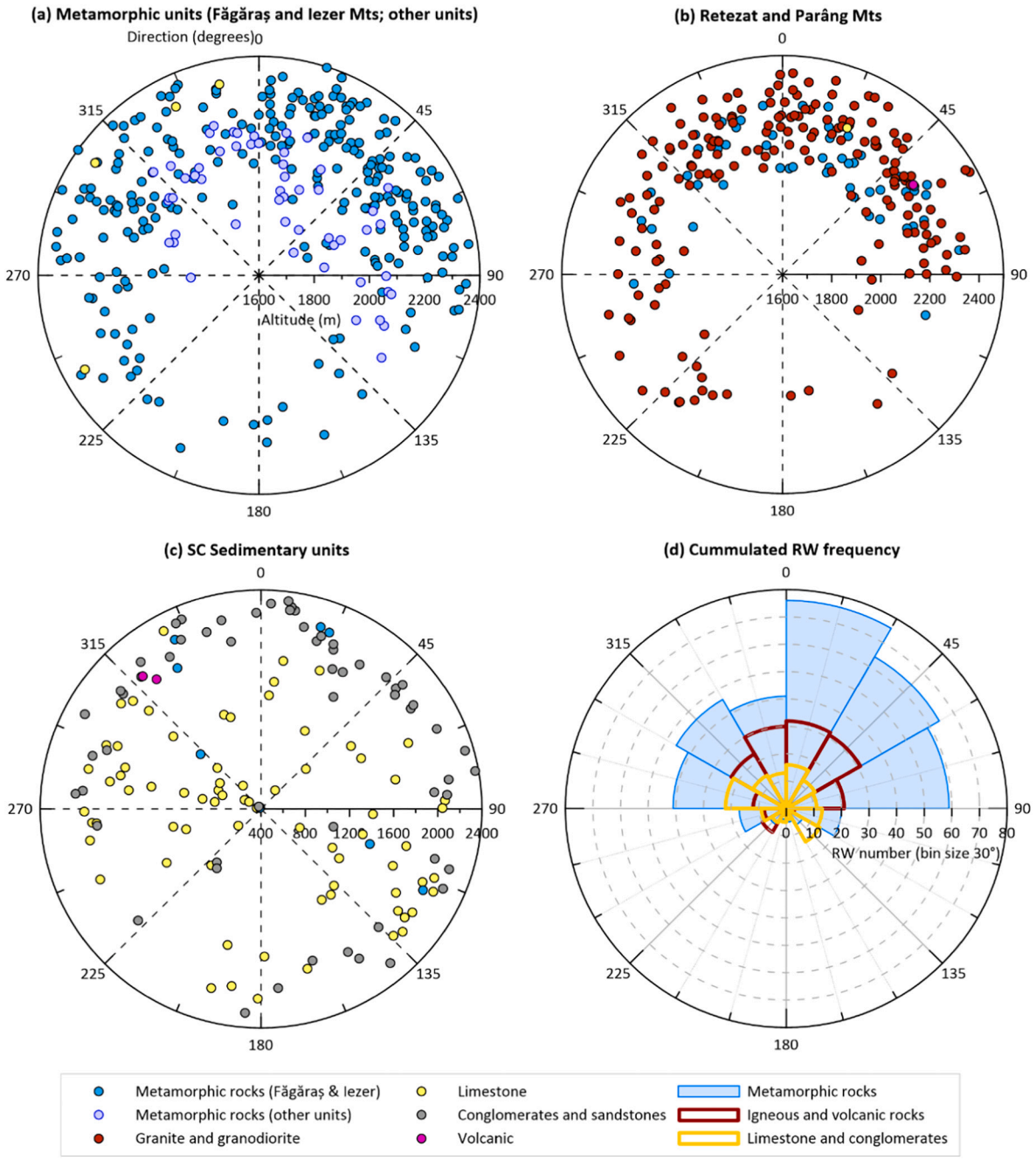

Fig. 5. Direction and mean altitude of the RW mapped in the SC: (a) Făgăraș and Iezer Mts., with the secondary cluster of RW mapped in the lower altitude SC metamorphic units; (b) distribution of igneous and metamorphic rock surfaces in Parâng and Retezat Mts.; (c) distribution of limestone, conglomerate and sandstone RW mapped in SC; (d) Cumulated RW distribution on the four main rock categories represented on 30° direction bins (please refer to the colour version).

amphibolite (metamorphic rocks representing 23 % of the mapped surfaces in the two massifs) (Tables 1, 2) (Fig. 5b). Approximately 54 % of the RW from Parâng and Retezat are North–oriented. Eastern and western exposures account for 25 % and 15 % of the total number, and 5.7 % of the mapped surfaces from the two massifs were identified on the southern slopes. More than half of the RW are concentrated in the 2100–2300 m interval and almost 18 % extend above 2300 m, the northern ones reaching the highest altitudes. The RW on metamorphic rocks in the two massifs range at slightly lower altitudes than in the igneous sectors and occur almost evenly on the East, North and West–oriented slopes.

In the limestone units from the SC, (Bădescu and Tîrlă, 2020), almost 40 % of the mapped RW are exposed towards West directions, 26 % to the East, 23 % are on northern slopes, and 11 % on the southern ones (Fig. 5c, d). In terms of altitudinal distribution, there are also major discrepancies between the massifs, the highest mean RW altitude being reached in Piatra Craiului (1970 m) (Table 1).

Bucegi is the highest sedimentary massif (2507 m) from the Carpathians, with most RW developed on conglomerates and sandstones, and 15 % on limestone outcrops. RW are distributed mainly on the northern slopes (37 %) and 16 % are South–facing. Maximum RW density is between 2100 and 2300 m for the North and East–exposed slopes. East, South and West RW are situated at lower elevations and occur on a wider altitudinal range (from 1800 to 2200 m).

The statistical analysis shows the clear dominance of West–exposed RWs for most of the considered morphometric parameters compared to

Table 3
Results of the statistical analysis (Post–Hoc Dunn's Test) of morphometric parameters for pairs of main exposures. Numbers represent the z-Score, which indicates whether the tested parameter pair has a value above the rank mean (positive value), or below (negative value). For example, the mean area of N/E pair has a z-Score = 2.38, meaning that North has a greater mean area than East. In a similar way, for z-Scores below the rank mean the comparison is read inversely, as in the altitude for S/N pair which has a z-Score = −6.05, meaning that North has a higher altitude than South.

Ratio	Mean area	Height	Altitude
N/E	2.38 (**)	2.36 (**)	3.19 (***)
S/E	1.11 (·)	1.33 (·)	−3.7 (***)
W/E	5.34 (***)	5.71 (***)	−2 (*)
S/N	−0.41 (·)	−0.17 (·)	−6.05 (***)
W/N	3.66 (***)	4.1 (***)	−5.27 (***)
W/S	2.76 (**)	2.83 (**)	2.18 (*)

A p–value < 0.05 indicates a strong statistical significance at 95 % confidence level.
· p-Value > 0.05.
* p–Value (0.05, 0.01].
** p–Value (0.01, 0.001].
*** p–Value < 0.001.

the other main orientations (Table 3). This asymmetry is however case–specific and imposed by the particular orientation of many of the sedimentary units, respectively the NNE–SSW–oriented ridges and plateaus of Piatra Craiului and Buila hogbacks, Bucegi, Ciucaș and Hășmaș synclines (Mutihac, 1990) or Cerna Valley half–graben (Povară et al., 2013), which together with the eastward and southward dipping strata contribute to the larger occurrence of West and North–exposed RWs.

In summary, our observations indicate that RW in metamorphic and igneous units are generally restricted to altitudes higher than 2100 m, show a high density on the North–exposed slopes and are almost absent from the southern ones. In comparison, RW distribution in sedimentary units is spread over a larger range of altitudes but highly dependent on the strata dip-direction which result in prevalent West and North exposures but not strongly asymmetric, which is the case for metamorphic and igneous rocks.

4.2. RW morphometry

Although the most numerous RW were identified on metamorphic and igneous rocks, these groups cover only 21 % and 12 % respectively from the total RW area mapped in the entire mountain range. Comparatively, although counting less RW, the sedimentary massifs in which limestone, conglomerates and sandstone prevail, cumulate 67 % of the total RW area in the EC and SC (Fig. 6a, b) measuring up to 5 times larger individual surfaces than igneous and metamorphic RW (Fig. 7a).

Metamorphic and igneous units are relatively similar in terms of RW vertical extension (around 70 m in average) and show little inter–site variation whereas RW in sedimentary units (limestone, conglomerate and sandstone) reach almost double height values (Figs. 6b, 7b). This visible heterogeneity is imposed by Bucegi and Piatra Craiului, with individual RW of up to 250 m height. This is also consistent with the wider range of mean RW altitude, limestone RW surfaces extending several hundreds of meters lower (Fig. 7c).

Summing up, the high values of the z-scores in Table 4 (maximum

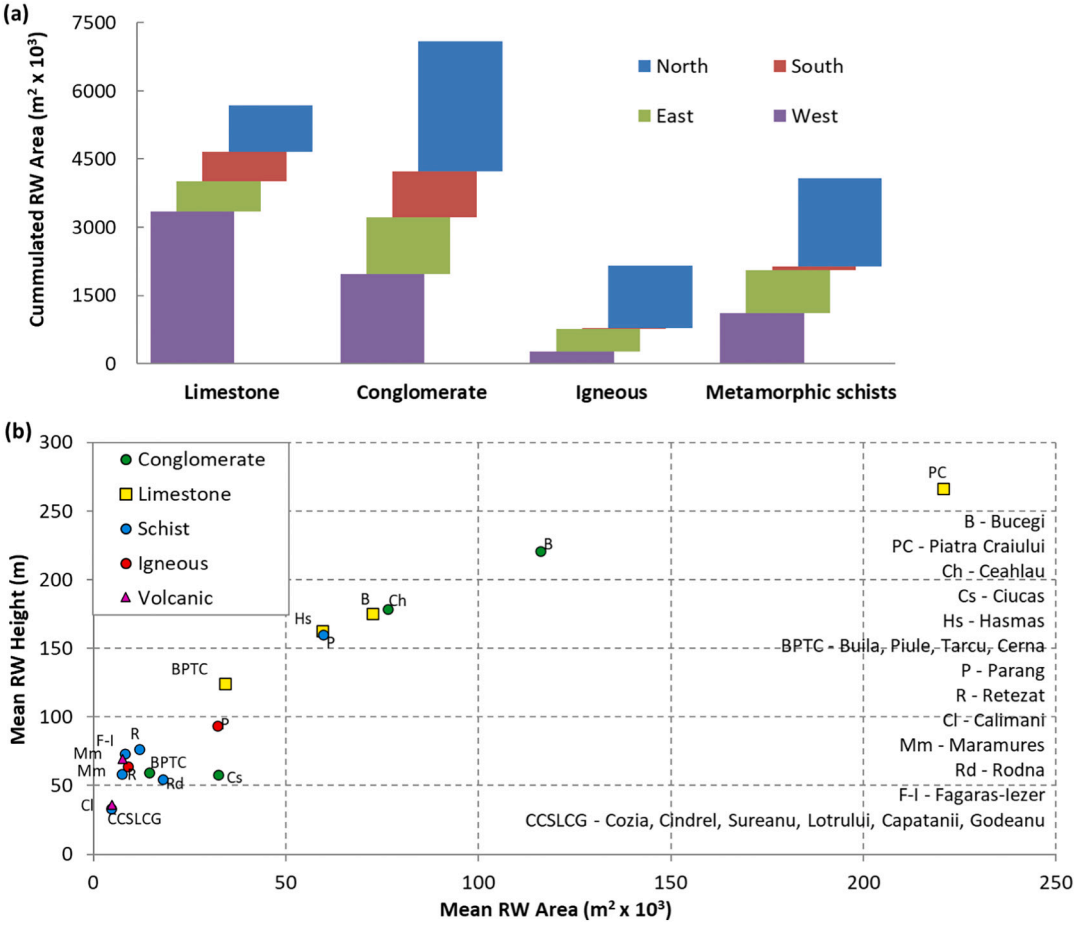

Fig. 6. General RW morphometry on the main rock types (counting all features from both EC and SC corresponding to the same rock type): (a) Cumulated area of RW surfaces with the same lithology grouped on the four main cardinal directions; (b) Mean RW height and area derived for each massif (please refer to the colour version).

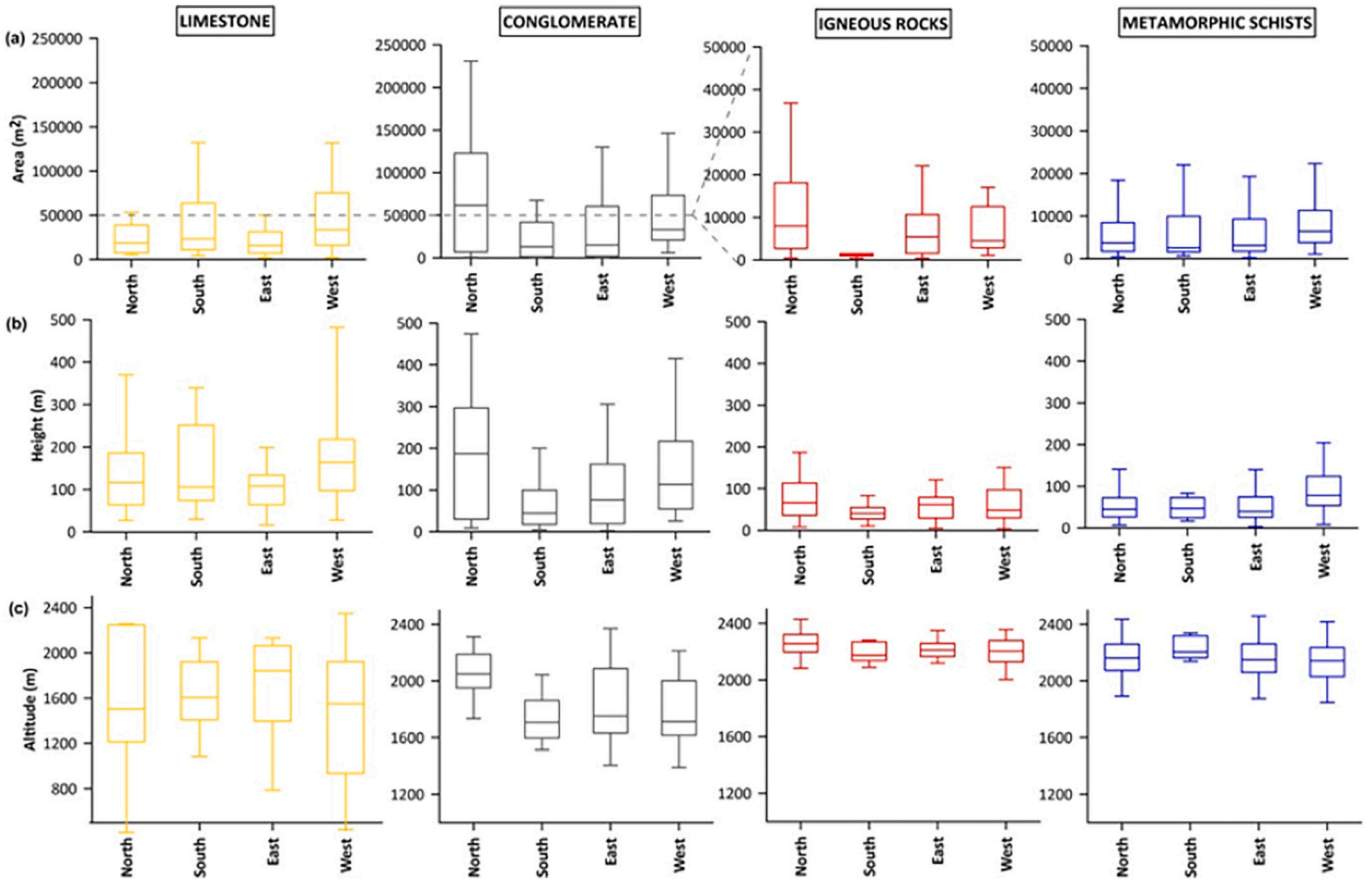

Fig. 7. Variability of the morphometry of the RW grouped in the main lithological classes in respect to the main orientations, averaged from individual values per lithology and aspect classes respectively: (a) mean RW area; (b) mean height; (c) mean altitude. The boxes display the median values, the 25–75 quartiles (lower – upper) and the caps show the minimum and maximum values (1.5 IQR).

Table 4
Results of the statistical analysis (Post–Hoc Dunn's Test) of morphometric parameters for pairs of main exposures. Numbers represent the z-Score, which indicates whether the tested parameter pair has a value above the rank mean (positive value), or below (negative value).

Ratio	Area	Height	Altitude
Conglomerate/limestone	−1.78 (*)	−3.9 (***)	2.93 (**)
Granite/limestone	−7.54 (***)	−6.9 (***)	12.89 (***)
Schist/limestone	−9.01 (***)	−8.36 (***)	10.9 (***)
Granite/conglomerate	−5.99 (***)	−2.79 (**)	10.31 (***)
Schist/conglomerate	−7.46 (***)	−3.87 (***)	7.91 (***)
Schist/granite	−0.77 (·)	−0.83 (·)	−4.53 (***)

A p–value < 0.05 indicates a strong statistical significance at 95 % confidence level.
· p-Value > 0.05.
* p–Value (0.05, 0.01].
** p–Value (0.01, 0.001].
*** p–Value < 0.001.

−9.01 for schist/limestone area, 10.9 for mean altitude) support the high morphometric differences that exist between the sedimentary units and the metamorphic and igneous ones, which share more similarities (−0.77 for schist/granite area, −4.3 for altitude). Although numerous, metamorphic and igneous RW in the study area are generally small–size rock surfaces perched to the upper part of formerly glaciated valleys and cirques. Both granite and schist RW in the study area are characterized by large joints networks (with metric-size surfaces in-between joints) which fit well with the dimensions of the boulders enclosed into the adjacent debris deposits (Vasile and Vespremeanu-Stroe, 2017a, 2017b), supporting the hypothesis of deep slope modelling by frequent and high magnitude rock falls which led to the formation of presently large debris deposits, talus cones and rock glaciers (Onaca et al., 2017a, 2017b). The sedimentary (limestone and conglomerates prevailing) RW are wider, steeper and cover larger areas than all the other lithological groups independent of glacial landmarks and with apparent homogeneity in respect to slope orientation. These characteristics thus reflect major differences between control factors over RW morphometry and distribution depending on geology, as we can associate present sedimentary RW high extent to the original structural uplift.

4.3. Absolute ages

Sample locations, altitudes, ^{10}Be concentrations and ^{10}Be surface exposure ages determined in this study and selected from the literature are presented in Table 5. Multiple values (3 to 5 per valley) available in 8 of the valleys presented here, allowed an intra and inter-massif analysis of age distributions. Values range between 0.97 ± 0.08 ka and 11.3 ± 1.0 ka (Table 5), clustering between 11.3 and 9.1 ka (21 values), thus closely following the Younger Dryas (12.6–11.4 ka, Tămaş et al., 2005; 12.9–11.7 ka, (Rasmussen et al., 2006) and within time lags of up to 2.6 ka after. A second high frequency cluster was found between 9.0 and 7.0 ka, while younger ages were identified with a frequency of 1.75 values/1000 yrs. There is not a clear correlation between the absolute ages of the rock surfaces and the altitude. Such an attempt would be hindered by the uneven spatial sample distribution, given the fact that most of the boulders are situated above 1800 m a.s.l. Nevertheless, most of the youngest ages (0.94 ± 0.08 ka, 4.51 ± 0.18 ka, 2.19 ± 0.12 ka, 1.27 ± 0.22 ka) were found in the lower or mid-sectors of Dejani, Bâlea and

Table 5
Sampling locations, ^{10}Be concentrations, and ^{10}Be surface exposure ages for post–Younger Dryas dated boulders in the Romanian Carpathians.

Location	Sample name	Lat (N)	Long (E)	Altitude (m)	Quartz mass (g)	[^{10}Be] atoms g^{-1} × 10^4	t (exposure time) ka	Source
Făgăraș								
Arpaș	AR01	45.5972	24.6656	2134	23.23	8.76 ± 0.33	4.07 ± 0.13	This study[a]
Bâlea Valley	BL	45.6391	24.6041	1205	24.39	4.92 ± 0.18	4.51 ± 0.18	
Dejani Valley	DEJ01	45.6062	24.9418	1300	23.05	1.13 ± 0.10	0.97 ± 0.08	
Dejani Valley	DEJ02	45.6072	24.9421	1287	26.72	8.15 ± 0.31	7.11 ± 0.26	
Dejani Valley	DEJ03	45.5876	24.9377	1929	26.00	16.91 ± 0.63	9.11 ± 0.34	
Dejani Valley	DEJ04	45.6009	24.9415	1401	25.77	13.36 ± 0.50	10.55 ± 0.39	
Fundul Caprei Valley	FC02A	45.5968	24.6429	1850	23.11	15.71 ± 0.59	9.04 ± 0.33	
Mioarele cirque	MIO01	45.5840	24.8341	2287	26.41	24.28 ± 0.91	10.14 ± 0.38	
Mioarele cirque	MIO02	45.5846	24.8340	2274	22.88	24.18 ± 0.76	10.14 ± 0.31	
Mioarele	MIO03	45.5842	24.8335	2285	24.74	24.33 ± 0.91	10.15 ± 0.38	
Orzăneaua cirque	ORZ02	45.6017	24.7235	1985	25.55	16.98 ± 0.64	8.79 ± 0.33	
Sâmbăta Valley	VS02	45.6119	24.7963	1823	25.11	16.60 ± 0.62	9.65 ± 0.36	
Sâmbăta Valley	VS01	45.6137	24.7957	1796	23.66	16.77 ± 0.57	9.95 ± 0.33	
Sâmbăta Valley	SA07	45.6361	24.7934	1215	26.22	2.46 ± 0.09	2.19 ± 0.12	
Sâmbăta Valley	SA05	45.6199	24.7909	1485	14.56	1.87 ± 0.07	1.27 ± 0.22	
Sâmbăta Valley	SA04	45.36	24.47	1820	–	–	10.00 ± 0.30	
Urlea cirque	U04	45.6017	24.8425	2077	25.44	16.00 ± 0.60	7.92 ± 0.29	
Urlea cirque	U01	45.5997	24.8358	2134	22.88	19.68 ± 0.59	9.36 ± 0.28	
Urlea cirque	U06	45.5960	24.8540	2062	27.87	22.14 ± 0.83	10.86 ± 0.40	
Urlea cirque	U01A	45.6001	24.8361	2130	23.07	22.94 ± 0.86	10.95 ± 0.41	
Doamnei RW N	DBEN	45.5952	24.6006	2230	20.48	3.59 ± 0.24	2.07 ± 0.13	
Doamnei RW S	DBES	45.5946	24.6008	2243	20.24	121.18 ± 2.06	52.46 ± 0.89	
Doamnei RG1	DBE1	45.6018	24.6035	2057	20.33	20.39 ± 0.94	9.91 ± 0.45	
Doamnei RG2	DBE2	45.6013	24.6026	2062	20.61	26.71 ± 0.79	12.97 ± 0.38	
Doamnei RG3	DBE3	45.6004	24.6027	2082	21.07	23.88 ± 0.71	11.44 ± 0.34	
Doamnei RG4	DBE4	45.5971	24.6016	2133	20.70	7.01 ± 0.22	3.37 ± 0.10	
Bucegi								
Gaura Valley	Gaura05	45.4387	25.4095	1541	25.41	15.76 ± 0.61	10.78 ± 0.43	
Gaura Valley	Gaura06	45.4383	25.4094	1545	25.74	15.50 ± 0.46	10.62 ± 0.33	
Gaura cirque	Gaura03	45.4417	25.4328	2072	15.44	15.72 ± 0.49	7.49 ± 0.23	
Gaura cirque	Gaura01	45.4420	25.4336	2081	25.39	15.60 ± 0.53	8.00 ± 0.25	
Parang								
Iezer Valley	PR01	45.34	23.63	2034	10.99	24.34 ± 1.08	11.20 ± 0.50	Gheorghiu et al. (2015)[b]
Iezer Valley	PR03	45.34	23.62	1970	14.33	13.61 ± 0.46	6.20 ± 0.20	
Iezer Valley	PR05	45.34	23.62	2008	10.6	19.64 ± 0.63	8.80 ± 0.80	
Gâlcescu cirque	PR10	45.35	23.61	1990	8.21	24.29 ± 0.69	11.20 ± 0.30	
Zănoaga Mare cirque	PR15	45.35	23.59	2055	10.19	23.63 ± 0.70	10.20 ± 0.30	
Zănoaga Mare cirque	PR16	45.35	23.59	2055	10.56	23.94 ± 0.83	10.40 ± 0.30	
Retezat								
Lăpușnicu Valley	Re15-29	45.3142	22.7803	1167	–	10.30 ± 0.13	10.70 ± 1.40	Ruszkiczay-Rüdiger et al. (2021)[c]
Pietrele Valley	Pt-03-02	45.28	22.88	1902	–	23.9	11.40 ± 1.30	Reuther et al. (2007)[d]
Rodna								
Pietroasă Valley	RD 30	47.61	24.64	1379	25.11	16.32 ± 0.50	10.50 ± 0.90	Gheorghiu (2012)[e]
Zănoaga Mare cirque	RD 04	47.6	24.64	1669	28.95	21.65 ± 0.63	11.50 ± 1.00	
Zănoaga Mare cirque	RD 06	47.6	27.63	1767	24.24	22.83 ± 0.63	11.30 ± 1.00	
Zănoaga Mare cirque	RD 07	47.6	27.63	1767	25.85	22.50 ± 0.65	11.10 ± 1.00	
Zănoaga Mare cirque	RD 05	47.6	27.63	1753	24.36	10.89 ± 0.40	5.70 ± 0.50	
Buhăiescu Valley	RD 19	47.58	24.65	1718	23.01	21.61 ± 0.63	10.40 ± 0.90	

[a] Analytical uncertainties (reported as 1-σ) included for all samples. No corrections for potential effects of snow cover or denudation were applied to the ages.
[b] Exposure ages calculated using Cronus-Earth ^{10}Be-^{26}Al exposure age calculator v. 2.2 (http://hess.ess.washington.edu/). They assume zero erosion, scaling factors according to Stone (2000) and a spallation production rate of 4.49 ± 0.39 atom (g SiO_2) −1 a-1 (Balco et al., 2008). Exposure ages are presented with the external uncertainties.
[c] The measured 10Be/9Be AMS ratios were corrected for full processed blank ratios: (3.30 ± 0.50) × 10^{-15}. Age uncertainties: the 1st number is the internal uncertainty (AMS measurement, weighting, carrier, blank and half-life; 1-σ). Every reported age was corrected for topographic- and self-shielding.
[d] Exposure age corrected for the effect of topographic shielding and surface geometry.
[e] Exposure ages calculated using Cronus-Earth ^{10}Be – ^{26}Al exposure age calculator v. 2.2 (http://hess.ess.washington.edu/). They assume zero erosion, scaling factors according to Stone (2000).

Sâmbăta valleys (Făgăraș Mts), between 1200 and 1500 m a.s.l., respectively. Although few ages from the onset of the Holocene were also determined below 1400 m in Retezat and Parâng Mts, (10.5 ± 0.9 ka, Gheorghiu et al., 2015; 10.7 ± 1.4 ka, Ruszkiczay-Rüdiger et al., 2021), most boulders dating between 11.5 and 7.0 ka are situated in the highest sector of the valleys and on cirque floors (1800–2200 m a.s.l.). This distribution pattern is similar when comparing both valleys within the same massif (e.g., Făgăraș) and valleys from the five different massifs (Table 5).

The samples from Doamnei rock glacier yielded values of 12.97 ± 0.38 in the front sector, which decrease to 9.91 ± 0.45 and 11.44 ± 0.34 ka in the middle part and 3.37 ± 0.10 ka at RW base. The exposure date of the source RW and the youngest rock glacier boulder age from the upmost sector indicate rockfalls activity during Late Holocene (Table 5). Comparatively, the South-exposed side of the ridge has returned a much older age (52.64 ± 0.89 ka).

5. Discussion

5.1. Climate, topography and lithology influence on RW distribution

The RW inventory and their morphometry have emphasized the differences imposed by the lithology on the characteristics of metamorphic, igneous and sedimentary RW in the Romanian Carpathians. We show that the first two rock categories produce much smaller RW, but developed at higher altitudes, than sedimentary massifs which account for the greatest RW cumulated area overall. Our results also showed that the distribution of RW in the Carpathians is very particular in respect to orientation, with an obvious asymmetry between North and South exposures especially for metamorphic and igneous rocks.

Despite the North/South balanced distribution of the glacial cirques (Mîndrescu, 2016), we found that RW have a high asymmetry in the metamorphic and igneous mountain units from the both EC and SC (Figs. 4a, 5b, d). South–exposed slopes are much less frequent while the total covered area (on these two rock categories) is almost 30 times higher on the North–exposed RW. Correspondently, rock glaciers distribution in the SC units accounts for 58 % of the mapped rock glaciers in the northern quadrant, and only 13 % in the southern one (Onaca et al., 2017b), which also suggests a more intense/frequent debris accumulation on the North exposed slopes during Younger Dryas and Early Holocene when presumably most of the rock glaciers formed (Onaca et al., 2013). A similar distribution is described in the Adamello–Presanella massif (Italian Alps), where the main ridge follows the NE-SW direction of the North-bordering fault and valleys radiate from the main ridge, covering all the cardinal directions. Here, based on the inventory of 216 rock glaciers mostly consisting of intrusive granodioritic and tonalitic rocks, Baroni et al. (2004) show that both active and relict rock glaciers are predominantly facing the North, NW and NE compared to the southern quadrant (which counts 18 % of the active/inactive, and 15 % of the relict ones), and argument, by comparing front altitudes, that local topoclimate makes northern slopes more favourable to rock glacier formation and preservation. We further consider that RW preservation conditions are also more restrictive on the southern slopes in igneous and metamorphic slopes, as commented below.

In a simulation of moisture availability in temperate alpine RWs, Rode et al. (2016) highlight that the preconditions of water saturation and temperature required for ice segregation are often recorded on the North-exposed slopes but are rarely met on warmer South–exposed rock surfaces, which implies that the latter are not prone for large–size debris production. Thus, South–exposed rock slopes would be subject to small–scale flake and granular rock shattering under the effect of both superficial freezing during snow melting intervals (Matsuoka, 2008) and of diurnal insolation thermal stress during snow–free intervals (Eppes et al., 2016). We assume that South–exposed RW in the Romanian Carpathians were generally less active in terms of dynamics than on other exposures yet producing small-fraction debris which cover the basal part of the rocky faces and favour soil development, thus contributing to the reduction in height and surface of the southern RW. This is also supported by the old age (52.46 ± 0.89 ka) yielded by the South-exposed ridge outcrop above Doamnei rock glacier, which was apparently unaffected by LGM, when it most probably stood as nunatak. Instead, we assume the North-exposed RW were most active in terms of RSF due to permafrost occurrence, deep seasonal frost and more humid conditions. Noteworthy, we estimate that permafrost covered most of the northern RW above 1500 m a.s.l. during Younger Dryas while its gradual degradation occurring in the Early Holocene generated a reactivation of the rock falls and rock-slope failures (Fig. 8). Humification process (i.e. humus formation in soil profiles) has been inferred to be more intense on South–exposed mountain slopes, where warmer conditions intensify oxidation and create a more optimal environment for microorganisms that degrade organic matter (Egli et al., 2010), compared to North–exposed mountain slopes which incorporate undecomposed or weakly degraded organic matter and are subject to mineral leaching due to colder and wetter conditions. Savi et al. (2015) reconstruct frost-cracking intensity and debris production during the Holocene in the Eastern Italian Alps, and emphasize that high debris accumulation occurred during Early Holocene and also during Atlantic and Subatlantic periods when positive MAAT would have promoted continuous superficial (up to 100 cm deep) frost cracking in the highest peaks (around 3000 m a.s.l.). A similar pattern is supported in the SC by the surface exposure ages that sustain production of large debris in all massifs during Early Holocene and secondary debris production in subsequent phases.

The cumulated effect of these processes could explain a generally faster cover with soil and vegetation on the sunny slopes of both metamorphic and igneous units from this study, whereas on the North, colder thermal regime and the production of large–size boulders led simultaneously to a better preservation of rock outcrops, which is reflected in present–day distribution and morphometry.

A different RW evolution pattern is inferred for the sedimentary units in the Romanian Carpathians, where RW formed in glacial cirques headwalls are not typical. The large synclines represented by Bucegi and Ciucaș Mts, with main North to South dip direction of the conglomerate and sandstones bedding planes uplifted large RW on the North–facing cuesta fronts, typical for sedimentary units formed as synclines, perched synclines, or hogbacks which are generally dominated by the compactness and steepness of the cuesta escarpments (Huggett, 2007). This is also the case in the NE–SW–dipping limestone massifs in SC which enhanced the development of the largest RW on their western slopes. Limestone RW in both EC and SC generally lack dense superficial joint networks which, along with increased permeability, limits water availability within the first centimetres of rock and implicitly turns ice segregation less probable, which further implies reduced RW modelling by frost shattering and debris accumulation in sedimentary massifs (Johnson et al., 2007). This is reflected by the low number of rock glaciers formed/identified in the SC on sedimentary rocks (only 15 on limestone from a total statistical population of 306 rock glaciers; Onaca et al., 2017a, 2017b). Therefore, we consider the lithology and tectonic uplift to play the major role in imposing the orientation–related homogeneity which accounts as the primary control in RW distribution and dimensions in the sedimentary units from this study. Secondary, postglacial RW relaxation would have led to the detachment of massive limestone and conglomerate blocks as sustained by the absolute ages obtained in Bucegi Mts (Table 5). However, in specific cases, such as the steep Piatra Craiului limestone hogback, large debris deposits have accumulated at the base of the main tectonic slopes. For such cases, we assume that the absence of transversal valleys and of the Pleistocene glaciers, both caused by topography, could have created the conditions for the long–term (e.g. Middle to Late Quaternary) debris accumulation, the formation of which is still to be deciphered.

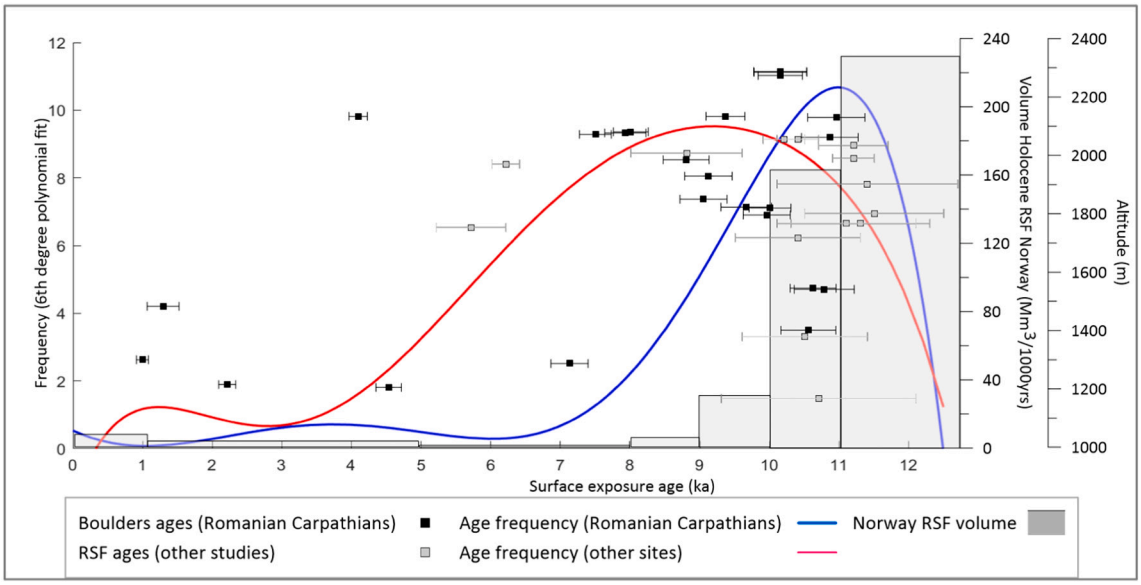

Fig. 8. Cumulated distribution of ^{10}Be surface exposure ages attributed to post-Younger Dryas RSF in the Romanian Carpathians (blue line), and multi-site composed RSF distribution (red line) using absolute ages from the French Alps (Cossart et al., 2008), Swiss Alps (Ivy-Ochs et al., 2009), Italian Alps (Hormes et al., 2008), Central Andes (Fauqué et al., 2009), Northern Iceland (Mercier et al., 2013), Central Karakoram (Shroder et al., 2011), Scotland and NW Ireland (Ballantyne et al., 2014). Grey-filled columns represent estimated volume of Holocene RSF in Norway (after Hermanns and Longva, 2013). (For interpretation of the references to colour in this figure legend, the reader is referred to the web version of this article.)

5.2. Holocene dynamics of RW depicted by rock-slope failures

Following post LGM deglaciation (19–14.5 ka), small glaciers re-occupied the highest cirques (> 2050–2100 m) during Younger Dryas excepting the southern ones (Gheorghiu et al., 2015; Popescu et al., 2017). Only the largest Younger Dryas glaciers are likely to have lasted as glacierets more than a millennium during Early Holocene (e.g. 10.2 ± 0.9 kyrs, Gheorghiu et al., 2015). Therefore, we consider that most of the boulders of early Holocene age dated in this study have originated by RW destabilization as response of ice retreat which occurred mainly in the upper valley/cirques sectors in which glaciers were restricted (Fig. 8). High frequency of such events occurring several thousand years after Younger Dryas period are well documented in the European Alps (Soldati et al., 2004; Cossart et al., 2008; Hormes et al., 2008; Prager et al., 2008; Ivy-Ochs et al., 2009), Tatra Mts (Pánek et al., 2016), in Scotland (Ballantyne et al., 2014) and Scandinavia (Mercier et al., 2013; Hilger et al., 2018, 2021; Vick et al., 2022), but also in Karakorum (Shroder et al., 2011) or the Andes (Fauqué et al., 2009). Many of these sites record re-activations or secondary clusters during the Sub-Boreal period (Hermanns and Longva, 2013).

In Fig. 8 we compare frequency curves of the post Younger Dryas boulders dated in the Romanian Carpathians and of the RSF ages compiled from these studies after excluding the mountain ranges which are influenced by excess of humidity/dryness and correspondently by their variability in time (e.g., Himalaya, Atlas or Cascade Mts). Overall, the Romanian Carpathians show a similar general trend with the other world-wide catenae but with an apparently more rapid and accentuated response to the Early Holocene warming and more humid conditions, so that almost ¾ of the dated RSF occurred before 8 ka with the highest frequency window positioned during 11.6–9 ka. Conversely, the multi-sites curve reflects a higher sensitivity of RW (deduced via RSF occurrence) to the Holocene Climatic Optimum, which can be explained both by delays in local deglaciation momentum and topoclimatic conditions. Given the relatively small number of samples used in our study (38), this first attempt to assess the RSF evolution in the Romanian Carpathians might also be biased towards the Early Holocene by the increased frequency of the high-altitude samples (71 % of the samples are >1700 m). As future research, it is necessary to expand the RSF dating by including more cases from the mid and low-altitude levels and to compare their histories in order to disentangle the influence of deglaciation, permafrost thawing, thermal and humidity variation. However, some of the European studies describe similar results with the newly-obtained in the Romanian Carpathians, such as Hermanns and Longva (2013) which give an estimation of Holocene RSF magnitude in Storfjörden, Norway, showing that the earliest events (12.5 to 10 kyrs) generated by far the largest detached volumes (Fig. 8), compared to the ones dating after 8 kyrs. Similarly, reconstructed magnitudes of large landslides from the Alps (Soldati et al., 2004; Ivy-Ochs et al., 2009), place such events in the first millennia of the Holocene.

Independently of the absolute exposure ages used to assess the RSF probability occurrence during Holocene, the other four surface ages from Doamnei rock glacier, in the central Făgăraș massif, indicate multiple phases of debris accumulation, and, in the same time, the high magnitude of early–Holocene debris production, which supplied at least the lower half of the rock glacier body, demonstrated by the rapid accumulation of massive boulders as well as their displacement between 12.97 and 9.91 ka ago (Fig. 9). RW permafrost decay would have further enhanced subsequent rockfall or rock avalanches of smaller magnitude during the following warm episodes of the Holocene as also described in the Swiss Alps by Nagelisen et al. (2015). The particularly large boulders in the lower half of Doamnei rock glacier are incompatible with frost-cracking intensities estimated for the Holocene (Savi et al., 2015) and were most probably produced by similar high magnitude (as described by Hermanns and Longva, 2013) slope failures induced by slope relaxation, permafrost degradation and overall weakened slope coherence. We consider this to be the ultimate process/interval of intense modelling in the alpine area of the Carpathians which defined the rock walls – rock glaciers/debris systems preserved until present.

6. Conclusions

The distribution of RW mapped in the Southern and Eastern Carpathians depends mainly on the lithology, structural predisposition but also weathering processes. In the metamorphic and igneous units, it ultimately relates to geomorphological context, being more likely associated with glacial cirques and valleys headwalls. Most schist and

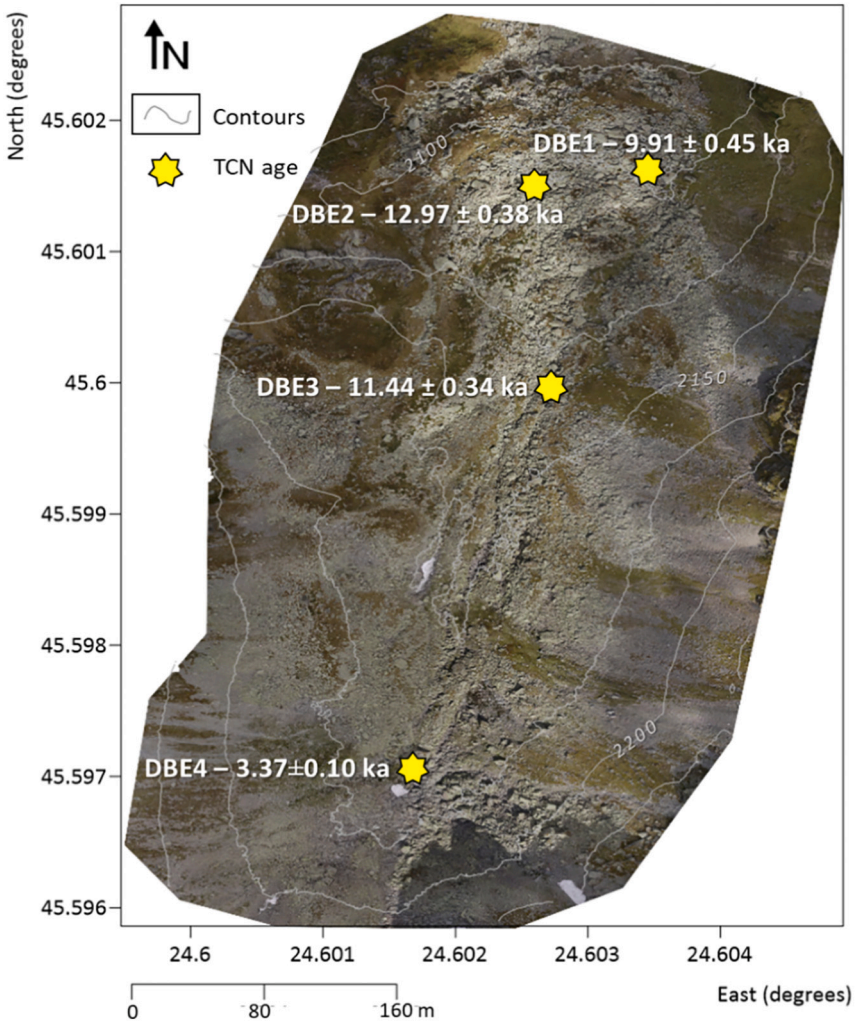

Fig. 9. Sampling locations and rock surface absolute ages on Doamnei rock glacier (central Făgăraș Mts).

granite RW are therefore restricted to the highest ridge sectors, while their reduced heights and mean areas are explained as a consequence of the lithological predisposition to debris production, especially in permafrost degrading conditions during warming phases of the Early Holocene. The North/South asymmetry in rock glaciers distribution (also signalled in other mid-latitude ranges) is reflected by the lack of South-exposed RW. We assume more stable conditions prone to fine debris and soil formation on the southern slopes due to insolation and warmer conditions.

For the sedimentary RW, tectonics and the geological structure are the main controls to explain the occurrence of the large (wide and high) limestone and conglomerate RW in the Romanian Carpathians. Except for Bucegi Mts, which were high and large enough to host complex glaciers during the last glaciation, most of the sedimentary units from SC and EC were not subject to glacial erosion during LGM due to either steep topography (e.g., hogback ridges) or lower altitude, although RW permafrost was probably widespread.

Absolute exposure ages confirm that an intense rock slope degradation via rock-slope failures took place in the Carpathian metamorphic and igneous units in Early Holocene, similar with other European sites, reaching the highest magnitudes 11.6–9 ka ago especially above 1800 m altitude. We associate the present distribution of RW with this periglacially-active period which was the last time of rock surfaces substantial reshape.

CRediT authorship contribution statement

AVS proposed the research, MV conducted the research and wrote the manuscript draft, AP performed the mapping and statistics analysis, DP and RB provided the absolute age values and contributed to the analysis of post-Younger Dryas rock walls degradation, ASTER Team did AMS machine maintenance, tunning, running and data processing, RP assessed the periglacial influence in rock walls shaping, BE contributed to the morphometry discussion and reviewed the manuscript draft, AVS provided final revision of the manuscript draft.

Declaration of competing interest

The authors declare that they have no known competing financial interests or personal relationships that could have appeared to influence the work reported in this paper.

Acknowledgements

The research financing these results received funding from the Norway Grants 2014–2021 (project code RO-NO-2019-0415/contract no. 30/2020), from University of Bucharest grants (project code C1.2. PFE-CDI.2021-587/contract number 41PFE/2021) and from the Research Institute of the University of Bucharest fellowship for young researchers (2018–2019 grants, awarded to MV).

The ASTER AMS national facility (CEREGE, Aix-en-Provence) is

supported by the INSU/CNRS, the ANR through the “Projets thématiques d’excellence” program for the “Equipements d’excellence” ASTER-CEREGE action and IRD.

References

Allen, S., Huggel, C., 2013. Extremely warm temperatures as a potential cause of recent high mountain rockfall. Glob. Planet. Chang. 107, 59–69. https://doi.org/10.1016/j.gloplacha.2013.04.007.

Ardelean, A.C., et al., 2017. Quantifying postglacial sediment storage and denudation rates in a small alpine catchment of the Făgăraș Mountains (Romania). Sci. Total Environ. 599–600 (March 2018), 1756–1767. https://doi.org/10.1016/j.scitotenv.2017.05.131.

Arnold, M., Merchel, S., Bourlès, D.L., Braucher, R., Benedetti, L., Finkel, R.K., Aumaître, G., Gottdang, A., Klein, M., 2010. The French accelerator mass spectrometry facility ASTER: Improved performance and developments. Nuclear Instruments and Methods in Physics Research Section B: Beam Interactions with Materials and Atoms 268 (11–12), 1954–1959. https://doi.org/10.1016/j.nimb.2010.02.107.

Bădescu, B., Tîrlă, L., 2020. Harta carstului din România, 2020. Exploratorii, Asociația speologică.

Balco, G., et al., 2008. In: A Complete and Easily Accessible Means of Calculating Surface Exposure Ages or Erosion Rates From 10 Be and 26 Al Measurements, 3, pp. 174–195. https://doi.org/10.1016/j.quageo.2007.12.001.

Ballantyne, C.K., et al., 2014. Enhanced rock-slope failure following ice-sheet deglaciation: timing and causes. Earth Surf. Process. Landf. 39 (7), 900–913. https://doi.org/10.1002/esp.3495.

Baroni, C., Carton, A., Seppi, R., 2004. Distribution and behaviour of rock glaciers in the Adamello-Presanella massif (Italian Alps). Permafr. Periglac. Process. 15 (3), 243–259. https://doi.org/10.1002/ppp.497.

Bartosch, T., Stüwe, K., Robl, J., 2017. Topographic evolution of the Eastern Alps: the influence of strike-slip faulting activity. Lithosphere 9 (3), 384–398. https://doi.org/10.1130/L594.1.

Borchers, B., et al., 2016. Geological calibration of spallation production rates in the CRONUS-Earth project. Quat. Geochronol. 31, 188–198. https://doi.org/10.1016/j.quageo.2015.01.009.

Braucher, R., et al., 2003. In situ produced 10Be measurements at great depths: implications for production rates by fast muons. Earth Planet. Sci. Lett. 211 (3–4), 251–258. https://doi.org/10.1016/S0012-821X(03)00205-X.

Braucher, R., et al., 2011. Production of Cosmogenic Radionuclides at Great Depth: A Multi Element Approach. https://doi.org/10.1016/j.epsl.2011.06.036.

Braucher, R., et al., 2015. Preparation of ASTER in-house 10Be/9Be standard solutions. Nucl. Instrum. Methods Phys. Res., Sect. B 361, 335–340. https://doi.org/10.1016/J.NIMB.2015.06.012.

Chmeleff, J., et al., 2010. Determination of the 10Be half-life by multicollector ICP-MS and liquid scintillation counting. Nucl. Instrum. Methods Phys. Res., Sect. B 268 (2), 192–199. https://doi.org/10.1016/j.nimb.2009.09.012.

Corona, C., Trappmann, D., Stoffel, M., 2013. Parameterization of rockfall source areas and magnitudes with ecological recorders: when disturbances in trees serve the calibration and validation of simulation runs. Geomorphology 202, 33–42. https://doi.org/10.1016/j.geomorph.2013.02.001.

Cossart, E., et al., 2008. Slope instability in relation to glacial debuttressing in alpine areas (Upper Durance catchment, southeastern France): evidence from field data and 10Be cosmic ray exposure ages. Geomorphology 95 (1–2), 3–26. https://doi.org/10.1016/j.geomorph.2006.12.022.

Curry, A.M., Morris, C.J., 2004. Lateglacial and Holocene talus slope development and Rockwall retreat on Mynydd Du, UK. Geomorphology 58 (1–4), 85–106. https://doi.org/10.1016/S0169-555X(03)00226-5.

Duca, S., et al., 2014. Feasibility of ice segregation location by acoustic emission detection: a laboratory test in gneiss. Permafr. Periglac. Process. 25 (3), 208–219. https://doi.org/10.1002/ppp.1814.

Dunn, O.J., 1961. Multiple comparisons among means. J. Am. Stat. Assoc. 56 (293), 52–64. https://doi.org/10.1080/01621459.1961.10482090.

Egli, M., et al., 2010. The effects of exposure and climate on the weathering of late Pleistocene and Holocene Alpine soils. Geomorphology 114 (3), 466–482. https://doi.org/10.1016/j.geomorph.2009.08.008.

Ellis, M.A., Barnes, J.B., 2015. A global perspective on the topographic response to fault growth. Geosphere 11 (4), 1008–1023. https://doi.org/10.1130/GES01156.1.

Eppes, M.C., et al., 2016. Deciphering the role of solar-induced thermal stresses in rock weathering. Bull. Geol. Soc. Am. 128 (9–10), 1315–1338. https://doi.org/10.1130/B31422.1.

European Environment Agency (EEA). ***. https://www.eea.europa.eu/data-and-maps/data/copernicus-land-monitoring-service-eu-dem.

Fauqué, L., Hermanns, R., Hewitt, K., Rosas, M., Wilson, C., Baumann, V., Lagorio, S., Di Tommaso, I., 2009. Mega-deslizamientos de la pared sur del cerro Aconcagua y su relación con depositós asignados a la glaciación Pleistocena. Revista de la Asociación Geológica Argentina 65 (4), 691–712.

Geological Institute of Romania. ***. https://geoportal.igr.ro/.

Gheorghiu, D.M., 2012. Available at:. In: Testing climate synchronicity between Scotland and Romania since the last glacial maximum, pp. 1–214 http://theses.gla.ac.uk/3362/.

Gheorghiu, D.M., et al., 2015. Deglaciation constraints in the Parâng Mountains, Southern Romania, using surface exposure dating. Quat. Int. 388 (March 2016), 156–167. https://doi.org/10.1016/j.quaint.2015.04.059.

Girard, L., et al., 2013. Environmental controls of frost cracking revealed through in situ acoustic emission measurements in steep bedrock. Geophys. Res. Lett. 40 (9), 1748–1753. https://doi.org/10.1002/grl.50384.

Gruber, S., 2007. In: A Mass-conserving Fast Algorithm to Parameterize Gravitational Transport and Deposition Using Digital Elevation Models, 43, pp. 1–8. https://doi.org/10.1029/2006WR004868.

Gruber, S., Hoelzle, M., Haeberli, W., 2004. Permafrost thaw and destabilization of Alpine rock walls in the hot summer of 2003. Geophys. Res. Lett. 31 (13), 1–4. https://doi.org/10.1029/2004GL020051.

Hales, T.C., Roering, J.J., 2007. Climatic controls on frost cracking and implications for the evolution of bedrock landscapes. J.Geophys.Res.: Earth Surf. 112 (2), 1–14. https://doi.org/10.1029/2006JF000616.

Hermanns, R.L., Longva, O., 2013. Rapid rock-slope failures. Landslides (January), 59–70. https://doi.org/10.1017/cbo9780511740367.007.

Hilger, P., et al., 2018. Multiple rock-slope failures from Mannen in Romsdal Valley, western Norway, revealed from Quaternary geological mapping and 10Be exposure dating. The Holocene 28 (12), 1841–1854. https://doi.org/10.1177/0959683618798165.

Hilger, P., et al., 2021. Permafrost as a first order control on long-term rock-slope deformation in (Sub-)Arctic Norway. Quat. Sci. Rev. 251, 106718 https://doi.org/10.1016/j.quascirev.2020.106718.

Hormes, A., et al., 2008. 10Be exposure ages of a rock avalanche and a late glacial moraine in Alta Valtellina, Italian Alps. Quat. Int. 190 (1), 136–145. https://doi.org/10.1016/j.quaint.2007.06.036.

Huggett, R.J., 2007. Fundamentals of Geomorphology. Routledge.

Hughes, P.D., Gibbard, P.L., Woodward, J.C., 2007. Geological controls on Pleistocene glaciation and cirque form in Greece. Geomorphology 88 (3–4), 242–253. https://doi.org/10.1016/j.geomorph.2006.11.008.

Iancu, S., 1970. Masivul Parâng. Studiu Geomorfologic. University of Bucharest.

Ivy-Ochs, S., et al., 2009. Surface exposure dating of the Flims landslide, Graubünden, Switzerland. Geomorphology 103 (1), 104–112. https://doi.org/10.1016/j.geomorph.2007.10.024.

Johnson, B.G., Thackray, G.D., Van Kirk, R., 2007. The effect of topography, latitude, and lithology on rock glacier distribution in the Lemhi Range, central Idaho, USA. Geomorphology 91 (1–2), 38–50. https://doi.org/10.1016/j.geomorph.2007.01.023.

Krautblatter, M., Funk, D., Günzel, F.K., 2013. Why permafrost rocks become unstable: a rock-ice-mechanical model in time and space. Earth Surf. Process. Landf. 38 (8), 876–887. https://doi.org/10.1002/esp.3374.

Kromer, R., 2017. Available at:. In: Identifying and Monitoring Rockfall Precursors Using Terrestrial Laser Scanning for Improved Rockfall Hazard Management, p. 313 https://qspace.library.queensu.ca/handle/1974/22765.

Kruskal, W.H., Wallis, W.A., 1952. Use of ranks in one-criterion variance analysis. J. Am. Stat. Assoc. 47 (260), 583. https://doi.org/10.2307/2280779.

Lifton, Z.M., et al., 2009. Influence of rock strength on the valley morphometry of Big Creek, central Idaho, USA. Geomorphology 111 (3–4), 173–181. https://doi.org/10.1016/j.geomorph.2009.04.014.

Linzer, H.G., et al., 1998. Kinematic evolution of the Romanian Carpathians. Tectonophysics 297 (1–4), 133–156. https://doi.org/10.1016/S0040-1951(98)00166-8.

Loye, A., Jaboyedoff, M., Pedrazzini, A., 2009. Identification of potential rockfall source areas at a regional scale using a DEM-based geomorphometric analysis. Nat. Hazards Earth Syst. Sci. 9 (5), 1643–1653. https://doi.org/10.5194/nhess-9-1643-2009.

Magnin, F., et al., 2015. Determination of warm, sensitive permafrost areas in near-vertical rockwalls and evaluation of distributed models by electrical resistivity tomography. J.Geophys.Res.Earth Surf. 120 (5), 745–762. https://doi.org/10.1002/2014JF003351.

Mațenco, L., 2017. Tectonics and Exhumation of Romanian Carpathians: Inferences from Kinematic and Thermochronological Studies. Landforms Dynamics and Evolution in Romania. Springer International Publishing, pp. 15–56.

Matsuoka, N., 2008. Frost weathering and rockwall erosion in the southeastern Swiss Alps: long-term (1994–2006) observations. Geomorphology 99 (1–4), 353–368. https://doi.org/10.1016/j.geomorph.2007.11.013.

Matthews, J.A., et al., 2018. Small rock-slope failures conditioned by Holocene permafrost degradation: a new approach and conceptual model based on Schmidt-hammer exposure-age dating, Jotunheimen, southern Norway. Boreas 47 (4), 1144–1169. https://doi.org/10.1111/bor.12336.

Merchel, S., et al., 2008. Towards more precise 10 Be and 36 Cl data from measurements at the 10 À14 level: influence of sample preparation. Nucl. Inst. Methods Phys. Res. B 266, 4921–4926. https://doi.org/10.1016/j.nimb.2008.07.031.

Merchel, S., Herpers, U., 1999. An update on radiochemical separation techniques for the determination of long-lived radionuclides via accelerator mass spectrometry. Radiochim. Acta 84, 215–219.

Mercier, D., et al., 2013. The Höfðahólar rock avalanche (sturzström): chronological constraint of paraglacial landsliding on an Icelandic hillslope. The Holocene 23 (3), 432–446. https://doi.org/10.1177/0959683612463104.

Merten, S., 2011. Thermo-tectonic evolution of a convergent orogen with low topographic build-up: exhumation and kinematic patterns in the Romanian Carpathians derived from thermochronology. Available at:. Vrije Universiteit Amsterdam https://research.vu.nl/en/publications/thermo-tectonic-evolution-of-a-convergent-orogen-with-low-topogra.

Messenzehl, K., Dikau, R., 2017. Structural and thermal controls of rockfall frequency and magnitude within rockwall–talus systems (Swiss Alps). Earth Surface Processes and Landforms 42 (13), 1963–1981. https://doi.org/10.1002/esp.4155.

Messenzehl, K., et al., 2017. Regional-scale controls on the spatial activity of rockfalls (Turtmann Valley, Swiss Alps) — a multivariate modeling approach. Geomorphology 287, 29–45. https://doi.org/10.1016/j.geomorph.2016.01.008.
Micu, D.M., et al., 2015. Climate of the Romanian Carpathians. https://doi.org/10.1007/978-3-319-02886-6.
Mîndrescu, M., 2016. Geomorfometria circurilor glaciare din Carpații românești. Editura Universității din Suceava.
Mîndrescu, M., Cristea, I.A., Hutchinson, S.M., 2010a. Bathymetric and sedimentological changes of glacial lake Ştiol, Rodna Masiff. Carpathian J. Earth Environ. Sci. 5 (1), 57–65.
Mîndrescu, M., Evans, I.S., Cox, N.J., 2010b. Climatic implications of cirque distribution in the Romanian Carpathians: palaeowind directions during glacial periods. J. Quat. Sci. 25 (6), 875–888. https://doi.org/10.1002/jqs.1363.
Mutihac, V., 1990. Structura geologică a teritoriului României. Editura Tehnică.
Mutihac, V., 2004. Gologia României. Editura Didactică și Pedagogică, București.
Nagelisen, J., et al., 2015. Post-glacial rock avalanches in the Obersee Valley, Glarner Alps, Switzerland. Geomorphology 238, 94–111. https://doi.org/10.1016/j.geomorph.2015.02.031.
National Agency for Cadastre and Land Legislation (ANCPI). ***. http://geoportal.ancpi.ro/geoportal/imobile/Harta.html.
Onaca, A., et al., 2013. Assessment of internal structure of periglacial landforms from southern carpathians (romania) using dc resistivity tomography. Carpathian J.Earth Environ.Sci. 8 (2), 113–122.
Onaca, A., et al., 2015. Near surface thermal characteristics of alpine steep rockwalls in the Retezat Mountains. Forum Geogr. XIV (2), 124–133. https://doi.org/10.5775/fg.2067-4635.2015.091.d.
Onaca, A., Urdea, P., et al., 2017a. Present-day periglacial processes in the alpine zone. In: Rădoane, M., Vespremeanu-Stroe, A. (Eds.), Landforms Dynamics and Evolution in Romania. Springer International Publishing, pp. 147–176. https://doi.org/10.1007/978-3-319-32589-7_7.
Onaca, A., Ardelean, F., et al., 2017b. Southern Carpathian rock glaciers: inventory, distribution and environmental controlling factors. Geomorphology 293, 391–404. https://doi.org/10.1016/j.geomorph.2016.03.032.
Onaca, A., et al., 2020. Assessment of permafrost conditions in the highest mountains of the Balkan Peninsula. Catena 185 (March 2019), 104288. https://doi.org/10.1016/j.catena.2019.104288.
Pánek, T., et al., 2016. Cosmogenic age constraints on post-LGM catastrophic rock slope failures in the Tatra Mountains (Western Carpathians). Catena 138 (March), 52–67. https://doi.org/10.1016/j.catena.2015.11.005.
Phillips, M., et al., 2017. Rock slope failure in a recently deglaciated permafrost rock wall at Piz Kesch (Eastern Swiss Alps), February 2014. Earth Surf. Process. Landf. 42 (3), 426–438. https://doi.org/10.1002/esp.3992.
Popescu, R., Urdea, P., Vespremeanu-Stroe, A., 2017. Deglaciation history of high massifs from the Romanian Carpathians: towards an integrated view. In: Landforms Dynamics and Evolution in Romania. Springer International Publishing, pp. 87–117. https://doi.org/10.1007/978-3-319-32589-7_5.
Povară, I., et al., 2013. Water flow system within the Cerna Valley graben structure (SW of the Southern Carpathians, Romania). In: International Symposium on Hierarchical Flow Systems in Karst Regions.
Prager, C., et al., 2008. Age distribution of fossil landslides in the Tyrol (Austria) and its surrounding areas. Nat. Hazards Earth Syst. Sci. 8 (2), 377–407. https://doi.org/10.5194/nhess-8-377-2008.
Rasmussen, S.O., Andersen, K.K., Svensson, A.M., Vinther, B.M., Clausen, H.B., Siggaard-Andersen, M.-L., Johnsen, S.J., Larsen, L.B., Dahl-Jensen, D., Bigler, M., Röthlisberger, R., Fischer, H., Goto-Azuma, K., Hansson, M.E., Ruth, U., 2006. A new Greenland ice core chronology for the last glacial termination. Journal of Geophysical Research 111, D06102. https://doi.org/10.1029/2005JD006079.
Reuther, A.U., et al., 2007. Late Pleistocene glacial chronology of the Pietrele Valley, Retezat Mountains, Southern Carpathians constrained by 10Be exposure ages and pedological investigations. Quat. Int. 164–165, 151–169. https://doi.org/10.1016/j.quaint.2006.10.011.
Rode, M., Schnepfleitner, H., Sass, O., 2016. Simulation of moisture content in alpine rockwalls during freeze–thaw events. Earth Surf. Process. Landf. 41 (13), 1937–1950. https://doi.org/10.1002/esp.3961.
Ruszkiczay-Rüdiger, Z., et al., 2021. Limited glacial erosion during the last glaciation in mid-latitude cirques (Retezat Mts, Southern Carpathians, Romania). Geomorphology 384, 107719. https://doi.org/10.1016/j.geomorph.2021.107719.
Săndulescu, M., 1984. Geotectonica României. Editura Tehnică.
Sauchyn, D.J., Cruden, D.M., Hu, X.Q., 1998. Structural control of the morphometry of open rock basins, Kananaskis region, Canadian Rocky Mountains. Geomorphology 22 (3–4), 313–324. https://doi.org/10.1016/S0169-555X(97)00083-4.
Savi, S., Delunel, R., Schlunegger, F., 2015. Efficiency of frost-cracking processes through space and time: an example from the eastern Italian Alps. Geomorphology 232, 248–260. https://doi.org/10.1016/j.geomorph.2015.01.009.
Seong, Y.B., et al., 2009. Rates of basin-wide rockwall retreat in the K2 region of the Central Karakoram defined by terrestrial cosmogenic nuclide 10Be. Geomorphology 107 (3–4), 254–262. https://doi.org/10.1016/j.geomorph.2008.12.014.
Shapiro, S.S., Wilk, M.B., 1965. An analysis of variance test for normality (complete samples). Biometrika 52 (3/4), 591. https://doi.org/10.2307/2333709.
Shroder, J.F., et al., 2011. The role of mass movements on landscape evolution in the Central Karakoram: discussion and speculation. Quat. Int. 236 (1–2), 34–47. https://doi.org/10.1016/j.quaint.2010.05.024.
Soldati, M., Corsini, A., Pasuto, A., 2004. Landslides and climate change in the Italian Dolomites since the Late glacial. Catena 55 (2), 141–161. https://doi.org/10.1016/S0341-8162(03)00113-9.
Stone, J.O., 2000. Air pressure and cosmogenic isotope production. J.Geophys.Res.Solid Earth 105 (B10), 23753–23759. https://doi.org/10.1029/2000JB900181.
Tămaş, T., Onac, B.P., Bojar, A.V., 2005. Lateglacial-Middle Holocene stable isotope records in two coeval stalagmites from the Bihor Mountains, NW Romania. Geol.Q. 49 (2), 185–194.
Urdea, P., 2000. Munții Retezat. Studiu Geomorfologic. Editura Academiei Române, București.
Van Der Hoeven, A.G.A., et al., 2005. In: Observation of Present-day Tectonic Motions in the Southeastern Carpathians: Results of the ISES/CRC-461 GPS Measurements, 239, pp. 177–184. https://doi.org/10.1016/j.epsl.2005.09.018.
Vaida, M., Verniers, J., 2005. Biostratigraphy and palaeogeography of lower Devonian chitinozoans, from east and west Moesia, Romania. Geol. Belg. 8 (4), 121–130.
Vasile, M., Vespremeanu-Stroe, A., 2017a. Thermal Weathering and Distribution of Mountain Rockwalls. Springer Geography. https://doi.org/10.1007/978-3-319-32589-7_8.
Vasile, Mirela, Vespremeanu-Stroe, A., 2017b. Thermal weathering and distribution of mountain rockwalls. In: Rădoane, M., Vespremeanu-Stroe, A. (Eds.), Landforms Dynamics and Evolution in Romania. Springer International Publishing, pp. 177–196. https://doi.org/10.1007/978-3-319-32589-7_8.
Vermeesch, P., 2007. CosmoCalc: an Excel add-in for cosmogenic nuclide calculations. Geochem. Geophys. Geosyst. 8 (8), 8003. https://doi.org/10.1029/2006GC001530.
Vespremeanu-Stroe, A., et al., 2012. Rock glacier activity in the Retezat Mountains, Southern Carpathians, Romania. Permafr. Periglac. Process. 23 (2), 127–137. https://doi.org/10.1002/ppp.1736.
Vick, L.M., et al., 2022. Evolution and temporal constraints of a multiphase postglacial rock slope failure. Geomorphology 398. https://doi.org/10.1016/j.geomorph.2021.108069.
Willett, S.D., 1999. Orogeny and orography: the effects of erosion on the structure of mountain belts. J.Geophys.Res.Solid Earth 104 (B12), 28957–28981. https://doi.org/10.1029/1999jb900248.